APTD-0678

CR-1-191

PB 201 737

FURTHER DEVELOPMENT OF THE PHOTOCHEMICAL SMOG MODEL FOR THE LOS ANGELES BASIN

FINAL REPORT

March 1971

A. Q. Eschenroeder
J. R. Martinez

Prepared for
Environmental Protection Agency
Air Pollution Control Office
Under Contract No. EHSD 71-22

GENERAL RESEARCH CORPORATION
P.O. BOX 3587, SANTA BARBARA, CALIFORNIA 93105

Reproduced by
NATIONAL TECHNICAL
INFORMATION SERVICE
Springfield, Va. 22151

66

The work upon which this publication is based was performed pursuant to Contract No. EHSD 71-22 with the National Air Pollution Control Administration, Environmental Health Service, Public Health Service, Department of Health, Education and Welfare.

PB-201 737

STANDARD TITLE PAGE FOR TECHNICAL REPORTS	1. Report No. APTD-0678	2. Govt. Accession No.	3. Recipient's Catalog No.

4. Title and Subtitle
Further Development of the Photochemical Smog Model for the Los Angeles Basin

5. Report Date
March 1971

6. Performing Organization Code

7. Author(s)
A. Q. Eschenroeder, J. R. Martinez

8. Performing Organization Rept. No.

9. Performing Organization Name and Address
General Research Corporation
P. O. Box 3587
Santa Barbara, California 93105

10. Project/Task/Work Unit No.

11. Contract/Grant No.
EHSD 71-22

12. Sponsoring Agency Name and Address
Environmental Protection Agency
Air Pollution Control Office
Air Pollution Technical Information Center
P. O. Box 12055
Research Triangle Park, N. C. 27709

13. Type of Report & Period Covered
Final

14. Sponsoring Agency Code

15. Supplementary Notes

16. Abstracts

Results of research conducted on the further development of an earlier diffusion model are presented. This work has resulted in a diffusion model with photochemistry that is applicable to pollutants that undergo chemical changes. The techniques used in this report have been advanced to the stage where they can be adapted to the planning and implementation of air pollution abatement measures. The photochemical description has been extended to account for varying ratios of nitrogen to hydrocarbon. Some hypotheses of carbon monoxide interactions have been tested. Descriptions are given also of numerical integration improvements, and of refinements in the meteorological realism of the model. Finally, the paper presents validation tests for Los Angeles basin data and the significance of the results are discussed in terms of future applications of the technique.

17. Key Words and Document Analysis. (a). Descriptors

Mathematical models
Photochemical reactions
Reaction rates
Equations
Meteorology
Hydrocarbons
Nitrogen oxides
Carbon Monoxide
Smog
Oxidizers
Chemical composition

17b. Identifiers/Open-Ended Terms

Los Angeles basin

17c. COSATI Field/Group 13B, 7E

18. Distribution Statement	19. Security Class (This Report)	21. No. of Pages
Unlimited	UNCLASSIFIED	66
	20. Security Class. (This Page) UNCLASSIFIED	22. Price

FORM NBS-857(1-70)

DISCLAIMER

This report was furnished to the Air Pollution Control Office by

General Research Corporation
P. O. Box 3587
Santa Barbara, California 93105

in fulfillment of Contract No. EHSD 71-22

CONTENTS

SECTION		PAGE
I	INTRODUCTION	1
	A. Perspectives on Modeling Needs	1
	B. Overview of Previous Contributions	1
	C. Advances Made in the Present Work	5
II	KINETIC IMPROVEMENTS IN THE PHOTOCHEMICAL DESCRIPTION	7
	A. Additional Oxidation Chains	7
	B. Influence of Initial Composition	14
III	MATHEMATICAL AND METEOROLOGICAL IMPROVEMENTS	21
	A. Application of Padé Approximants to Smog Chamber Calculations	22
	B. Application of Padé Approximants to the Atmospheric Model Equation	26
	C. Meteorological Reformulation of Model	30
IV	TESTS OF THE MODEL AGAINST LOS ANGELES BASIN DATA	38
	A. Objectives of the Tests	38
	B. Review of the Previous Validation Study	38
	C. Sensitivity Studies on 1969 Trajectories with the Expanded Model	40
	D. History Analysis of the 1030 El Monte Trajectory	45
V	CONCLUDING REMARKS	51
	REFERENCES	57

ILLUSTRATIONS

NO.		PAGE
1	Schematic of Diffusion Model for Air Pollution Simulation	4
2	Expanded Kinetic Mechanism	9
3	Computed Curves Compared With Experimental Points	12
4	Hydrocarbon Decay With Two Reactivities	15
5	Ozone Buildup With Two Reactivities	16
6	Influence of NO_x:HC-Ratio on Oxidant Production	17
7	Estimated Trajectory of Air Mass Arriving at El Monte, 1030 hours, 29 Sept. 1969	33
8	Estimated Trajectory of Air Mass Arriving at El Monte, 1130 hours, 29 Sept. 1969	34
9	Estimated Trajectory of Air Mass Arriving at El Monte, 1230 hours, 29 Sept. 1969	35
10	Estimated Trajectory of Air Mass Arriving at El Monte, 1330 hours, 29 Sept. 1969	36
11	High Reactivity Hydrocarbon Concentration at Huntington Park on Type 2 Days, 1968. f = 1/4; r = 1/2	39
12	Ozone Concentration at Huntington Park on Type 2 Days, 1968. f = 1/4; r = 1/2	41
13	Reactive Hydrocarbon History Along the 1030 Trajectory. f = 1/4; r = 1/2 (Ground level concentrations)	46
14	Nitric Oxide History Along the 1030 Trajectory. f = 1/4; r = 1/2 (Ground level concentrations)	47
15	Nitrogen Dioxide History Along the 1030 Trajectory. f = 1/4; r = 1/2 (Ground level concentrations)	47

ILLUSTRATIONS (Cont.)

NO.		PAGE
16	Oxides of Nitrogen ($NO + NO_2$) History Along the 1030 Trajectory. f = 1/4; r = 1/2 (Ground level concentrations)	48
17	Ozone History Along the 1030 Trajectory. f = 1/4; r = 1/2 (Ground level concentrations)	50

I. INTRODUCTION

A. PERSPECTIVES ON MODELING NEEDS

Control of emission sources and of future land use offer possibilities for managing air quality. Under statutory mandate, regional implementation plans must be submitted to show how these controls will be applied. Mathematical models that give estimates of air quality in terms of emissions in a particular airshed should play a key role in formulating the plans.

The work described in this report has resulted in a diffusion model with photochemistry that is applicable to pollutants that undergo chemical changes. Although our further development of an earlier model[1] is still confined to the Los Angeles basin data, the method is applicable to the broad class of problems. Most of the pollutants covered by criteria documents participate in some forms of chemical reaction on time scales comparable with air residence times in urban areas. To account for this we have retained both the meteorology effects of dispersion and advection coupled with photochemical effects of primary pollutants producing oxidant compounds.

B. OVERVIEW OF PREVIOUS CONTRIBUTIONS

Since literature reviews[2,3,4] of air pollution modeling in general are available, our remarks here are confined to the previous work that was specifically directed toward reactive pollutants. The discussion centers on the relationship between the details emphasized by the model and the levels of precision in either input or output data. At the very least, any model must include the physics and chemistry of the governing phenomena, but complexities which far exceed reasonable expectations of specific validation are probably unjustified. In abstract language this says that we can fit any observed data by using enough adjustable parameters in the model, but that we leave the realm of physics if we do not subject most of the parameters to independent experimental verification.

The models described by Calvert[5] and Wayne, et al.,[6] stress chemical kinetic mechanism. In the former, the photochemical smog mechanism is reduced to 17 steps and in the latter to 31 steps. In the larger mechanism care is taken to describe plausible reaction for the C_3H_6/NO_x/air system, but it is ultimately applied to the atmospheric case where dozens of smog-forming hydrocarbons are involved. To preserve a consistent level of detail, the number of reactions must be increased by a large factor; however, this is avoided by adjusting the rate constants to obtain observed results. Homogeneously stirred air parcels following wind trajectories are assumed in order to retain first-order, ordinary differential equations.

Another way of restricting the mathematical complexity to first-order, ordinary differential equations is given in Friedlander and Seinfeld's paper.[7] This method reduces the chemical system to seven functional steps to be consistent with the level of observational detail usually available for polluted atmospheres.* Unlike the models discussed above, this one accounts for finite rate atmospheric diffusion. Retention of the mathematical simplicity is bought at the price of imposing the Lagrangian similarity hypothesis. This means that the vertical profiles of concentration in the polluted layer belong to simple parametric families. Careful choice of the profile form functions may well allow this method to be a fast and powerful computational tool.

Three-dimensional, time-dependent methods[8,9] have been proposed recently, but results for reactive atmospheres have not been reported at this writing. Simplified chemistry must be employed in each of these approaches because of the emphasis on details of advection and diffusion. The body of meteorological data for most air basins falls far short of the input requirements for any transport formulation of this complexity. Here again it is difficult to avoid the problem of allowing too many

*Even if more detail were included, there are no measured data on rate constants for most of the additional reactions. Consequently, the model is provided with additional degrees of freedom "wherever the kinetic data are open to estimation".

unspecified parameters to obscure the physically based portions of the calculation. One of the new methods employs an Eulerian coordinate frame which introduces the chronic problem of artificial (or numerical) diffusion. Small time and space steps are the only means suggested heretofore to remedy this problem. The other method uses a discretized representation of species concentrations in a Lagrangian frame. For multicomponent systems, the latter type of approach has previously been limited because of the large quantity of rapid access memory storage needed for each species. Both of these problems have been recognized for some time with three-dimensional, time-dependent calculations. More powerful computers and novel algorithms may well hold their solutions.

The method developed at General Research Corporation is more modest in its chemical detail than the models first described above, and it is far simpler in its transport formulation than the three-dimensional, time-dependent approaches. An attempt has been made to keep the mathematical descriptions near the level of detail and precision of observational data. This has resulted in a lumped-parameter, chemical kinetic mechanism and a Lagrangian air parcel with finite-rate vertical diffusion. The chief advantages of this over the approach of Ref. 7 are complete flexibility in specifying vertical diffusion and in accounting for distributed emission sources.

Our approach avoids the artificial numerical diffusion problem by the choice of natural (or so-called "intrinsic") coordinates. We align the coordinate system with the natural airflow at each instant so that there is practically no advection across any grid line. This permits us to follow air masses, to include vertical dispersion, and to account for chemical changes simultaneously. Figure 1 schematically illustrates these points. The large memory requirements do not appear in our approach because we trace the history point-by-point and output the results sequentially. Balancing the needs for realistic chemical and meteorological descriptions against efficiency of calculation, the GRC model has achieved

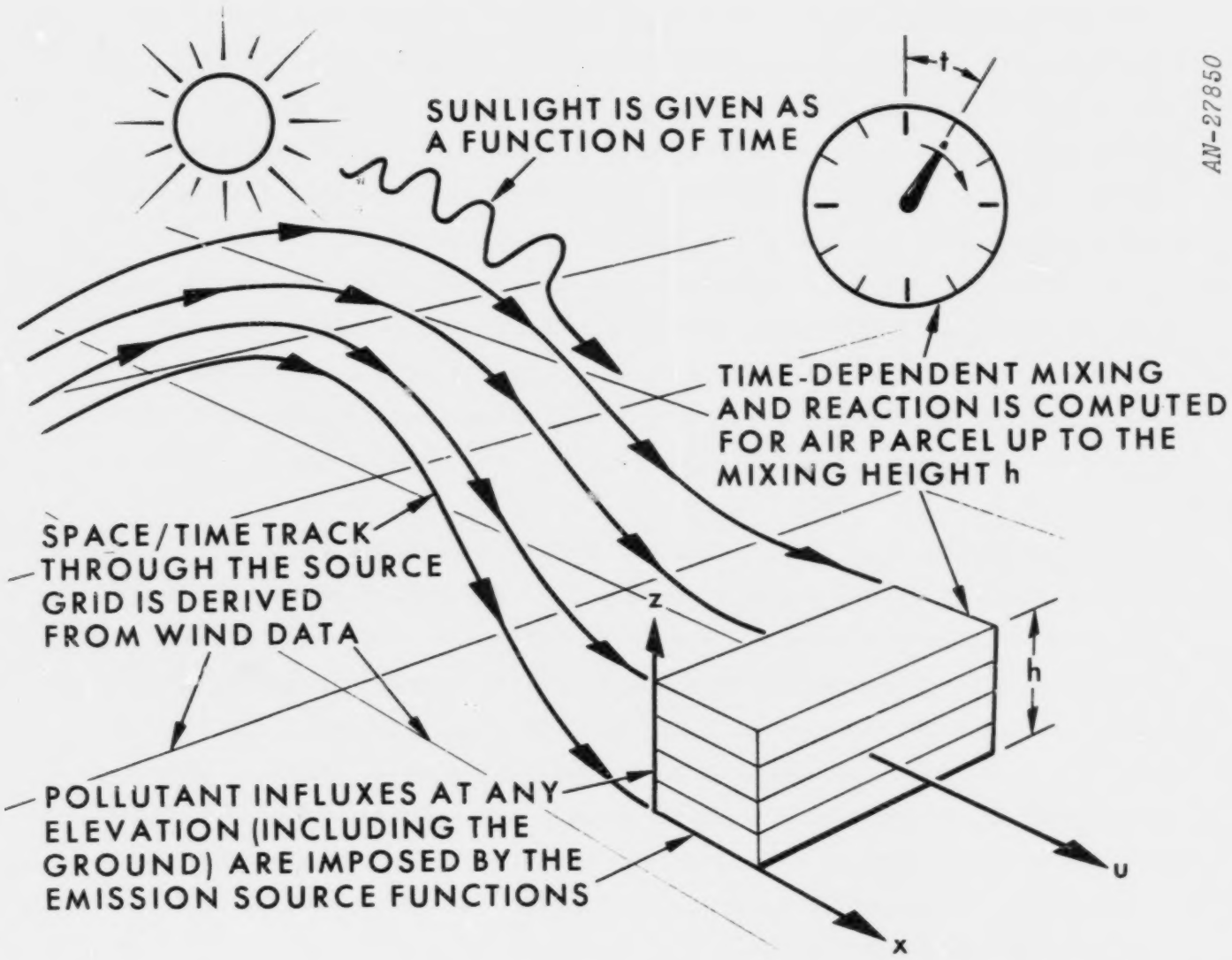
SUNLIGHT IS GIVEN AS A FUNCTION OF TIME
t
AN-27850
TIME-DEPENDENT MIXING AND REACTION IS COMPUTED FOR AIR PARCEL UP TO THE MIXING HEIGHT h
SPACE/TIME TRACK THROUGH THE SOURCE GRID IS DERIVED FROM WIND DATA
z
h
POLLUTANT INFLUXES AT ANY ELEVATION (INCLUDING THE GROUND) ARE IMPOSED BY THE EMISSION SOURCE FUNCTIONS
u
x

Figure 1. Schematic of Diffusion Model for Air Pollution Simulation

---

many of the scientific and practical objectives that it was designed for. It has not concentrated on the details of a specific hydrocarbon-nitrogen oxide system, but it has included the major atmospheric phenomena affecting transport and dispersion. Probably the most valuable factor in assuring its success is the constant contact with laboratory and atmospheric measurements. This exposure to realism prevents excursions into abstract chemical or mathematical hypotheses. Conversely, simple curve-fitting of specific atmopsheric data is avoided to retain generality.

It is useful to digress here to examine the relative magnitude of the horizontal diffusion terms which are neglected. Carbon monoxide will be chosen because it undergoes negligible atmospheric reaction over time scales of interest. We shall form a ratio taken from the CO-balance on the moving air parcel. The ratio of CO-loss horizontally to CO-gain vertically gives a measure of how serious our assumption is. The air parcel is taken to be 9 km^2 in horizontal area because this approximates the spatial resolution of the source grid. The vertical dimension is taken to be 100 meters, typical of a high pollution day. In order to force a high value for the ratio, the time of 1000 hours PST is selected because the numerator of the ratio is high (the air having just been loaded up by morning traffic) and the denominator is low (peak traffic has passed). Horizontal loss is the turbulent diffusion coefficient ($\sim$300 m^2/min) times the average crosswind gradient ($\sim 3.8 \times 10^{-10}$ mass fractions per meter) times the area of all four sides (1.2×10^6 m^2). The horizontal gradient is maximized by using a concentration decrement equal to the highest 10 A.M. reading in Huntington Park in 1969, which was 19 ppm. The characteristic distance over which the concentration drops from 19 ppm to zero is taken as the order of 30 miles. This gives a loss of about 0.1 m^3/min. Using a grid square in the central basin (containing both freeway and surface street contributions), we get a gain of about 20 m^3/min averaged over the 9-km^2 area. Consequently, the error committed is of the order of 0.5% in the CO-mass balance. We consider this to be a high estimate for the reasons outlined above.

C. ADVANCES MADE IN THE PRESENT WORK

Following the philosophy expressed above, we have advanced our techniques to the stage where they can be adapted to planning and implementation of air pollution abatement measures. As described in the next section, the photochemical description has been extended to account for varying ratios of oxides of nitrogen to hydrocarbon. Some hypotheses of carbon monoxide interactions have been tested. These kinetic improvements add several reaction steps to our previously adopted mechanism. With no

changes in numerical methods, the costs in computing time would have grown roughly in direct proportion.

Numerical integration improvements have more than offset the increases in chemical complexity. Another section describes these along with refinements in the meteorological realism of the model. The moving element shown in Fig. 1 replaces our previous formulation which was limited either to a horizontally uniform slab or a two-dimensional Eulerian coordinate system. The increased computing efficiency applies to both the homogeneous (smog chamber) and the diffusion (atmospheric) runs because we generalized it to apply to partial differential equations.

In the final sections of the paper, validation tests are presented for Los Angeles basin data and the significance of the results are discussed in terms of future applications of the technique.

II. KINETIC IMPROVEMENTS IN THE PHOTOCHEMICAL DESCRIPTION

A. ADDITIONAL OXIDATION CHAINS

It has been known for some time that hydrocarbon consumption rates observed in chamber experiments cannot be explained by ozone and oxygen atom attack alone. This is discussed in the review by Altshuller and Bufalini[10] where it is noted that Schuck and Doyle[11] termed the disparity an "excess rate." Our previous modeling work treated this by increasing both the O_3 and O-atom rates of reaction with hydrocarbon.

To use known rate constants to a maximum extent in the present work, we have added a hydrocarbon oxidation chain to reflect the attack of RO upon the hydrocarbon. Because of its suspected dominance,[12,13] the hydroxyl radical (OH) was assumed to be the only RO reacting with the hydrocarbon.

Following the inorganic cycle formed by

$$\left.\begin{aligned} h\nu + NO_2 &\rightarrow NO + O \\ O + O_2 + M &\rightarrow O_3 + M \end{aligned}\right\} \quad (1)^*$$

$$NO + O_3 \rightarrow NO_2 + O_2 \quad (2)$$

we have allowed each hydrocarbon oxidation to generate multiple RO_2 radicals as expressed by the b-factors in the steps

$$O + HC \rightarrow b_1(RO_2) \quad (3)$$

---

*The two reaction steps bracketed by (1) are combined by assuming O-atom stationarity internal to the logic of the computer program. Hence reaction (1) nets the system $h\nu + NO_2 \rightarrow NO + O_3$.

$$OH + HC \rightarrow b_2(RO_2) \tag{4}$$

$$O_3 + HC \rightarrow b_3(RO_2) \tag{5}$$

Subsequent conversion of NO to NO_2 was assumed to occur via

$$RO_2 + NO \rightarrow NO_2 + d(OH) \tag{6}$$

where d expresses that fraction of the conversion responsible for returning hydroxyl to the system.

Note that reactions (4) and (6) form something of a closed loop and that a stability requirement like $b_2 d < 1$ may be needed to prevent RO_2-runaway. This is not a precise requirement because of the variety of external factors that influence the flow rate of free radicals around the loop. Some of the RO_2 is formed by the other two reactions, and there are radical removal processes in the chain termination steps we discuss in the following paragraph.

Both RO_2 and OH are held in check by removal steps that terminate the chains. We continue to use some lumped parameter reactions such as

$$RO_2 + NO_2 \rightarrow c(PAN)^* \tag{7}$$

and some elementary reactions like

$$OH + NO + M \rightarrow HONO + M \tag{8}$$

$$OH + NO_2 + M \rightarrow HNO_3 + M \tag{9}$$

This rounds out the mechanism we have called Mark XII. It is diagrammed on Fig. 2.

---

*PAN is used to denote peroxyacetylnitrate.

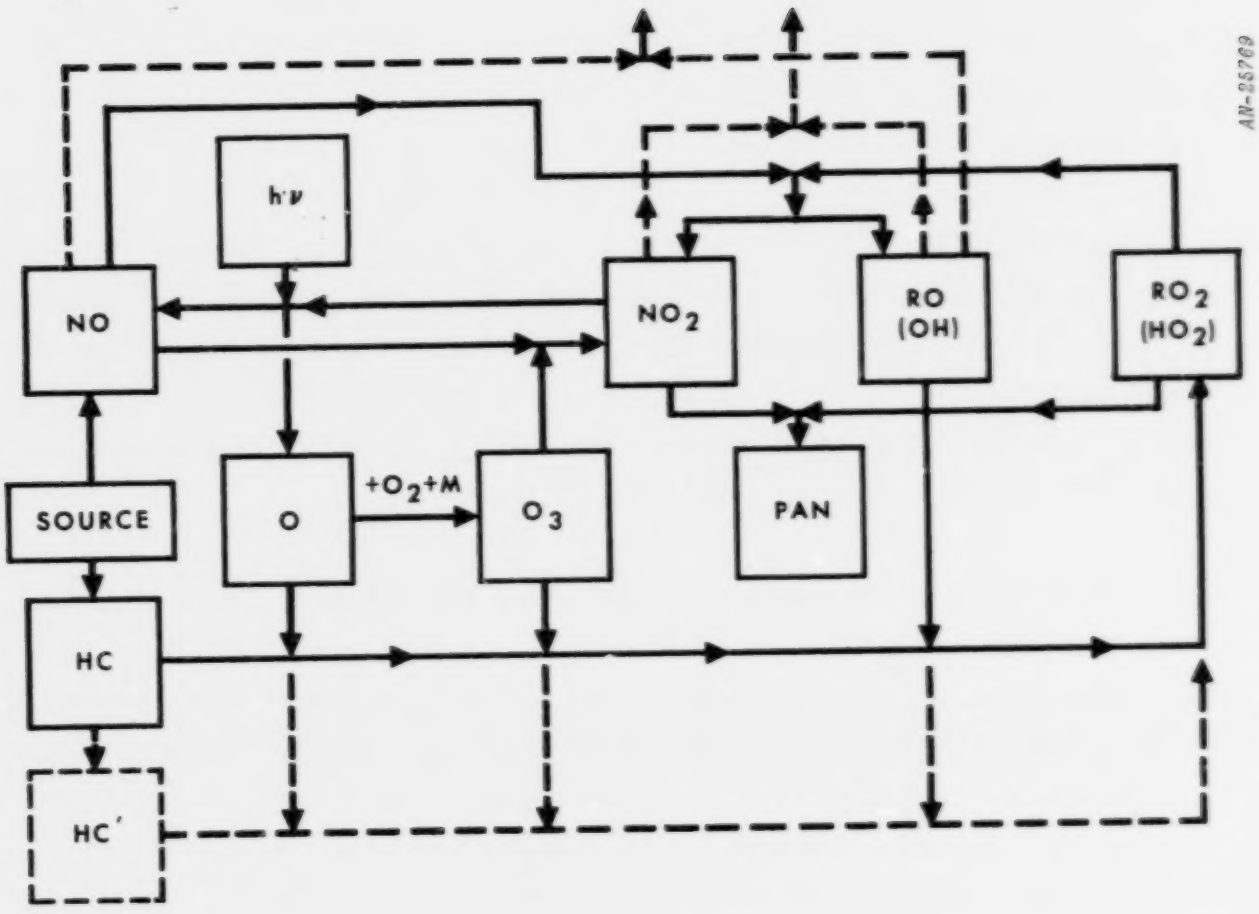

Figure 2. Expanded Kinetic Mechanism

In summary, the main changes from the previous scheme[1] are: addition of radical species RO (treated as OH), the provision for a multiplicity of hydrocarbons (not shown in equations), and the elimination of ozone production from an RO_2 reaction. The multiplicity of hydrocarbons is done by adding parallel reactions to (3), (4), and (5). The omission of the ozone production reaction is justified on the basis of its suspected endothermicity.[14]

For our initial validation tests we tried the rate constants compiled and estimated by Westberg and Cohen.[14] Stoichiometric coefficients b_1, b_2, and d were determined by hand-calculation analysis of some of the propylene data represented by Ref. 15. We found that $bd \simeq 1$ where b is a composite branching factor, and $b \simeq 2$ in order to explain the decay rate of NO compared with that of propylene.

Explosions of RO_2-concentration characterized some early choices of bd-combinations because of the positive feedback loop involving radical reactions shown in Fig. 2. Since these occurred in the first few seconds of real time, they were difficult to detect. Our usual printing interval of 1 minute of real time gave computer outputs showing sudden drops of NO and HC (to some nonzero levels) during the first minute followed by the dynamic equilibrium between NO, NO_2, and O_3 with a slow decay of hydrocarbon. The underlying pathology was discovered by rerunning with special diagnostic outputs.

Nominal rate constants were adjusted to reconcile computed results with measured values. For example, the (OH + HC)-rate was cut to abcut one-third the estimated value and the ($NO + RO_2$)-rate was increased eightfold. Reaction rates which have been reported individually in the literature were held at their nominal values including the (O + HC)-rate which we had to increase many-fold in previous work.[1] Also, the retention of reaction (5) was still necessary to describe the continued C_3H_6-decay after the near disappearance of NO.

In order to reproduce the late-time behavior of NO_2 and propylene, we included chain termination reactions in addition to those indicated in Fig. 2. In their more recent review,[16] Altshuller and Bufalini point out that HONO might be formed by the reaction with water vapor

$$NO + NO_2 + H_2O \rightarrow 2HONO \tag{10}$$

which is likely to proceed in the two steps

$$NO + NO_2 \rightarrow N_2O_3 \tag{11}$$

$$N_2O_3 + H_2O \rightarrow 2HONO \tag{12}$$

A possible source of OH-radical[12,13] is the photodissociation of HONO

$$h\nu + HONO \rightarrow OH + NO \tag{13}$$

Figure 3 shows the computed concentration history using this scheme to describe the experimental observations of Altshuller, et al.,[15] and Table 1 summarizes the reaction rate constants that were used. The column in Table 1 labeled "nominal" gives the values we started from on the basis of tabulations in Ref. 14. Following an empirical procedure, our calculations effectively combined H_2O-concentrations with the rate constant for reaction (10) as indicated; therefore no comparable nominal value is shown. Higher levels of precision than that shown in Fig. 3 were not among our objectives, since a detailed investigation of propylene is not justified for describing the potpourri of hydrocarbons in the urban atmosphere. Orders of magnitude for conversion times and levels are sufficiently good to proceed from here. The objective that we have fulfilled is to represent the so-called "excess rate" of hydrocarbon oxidation with added reactions instead of artificially increasing the O-atom rate with hydrocarbon.

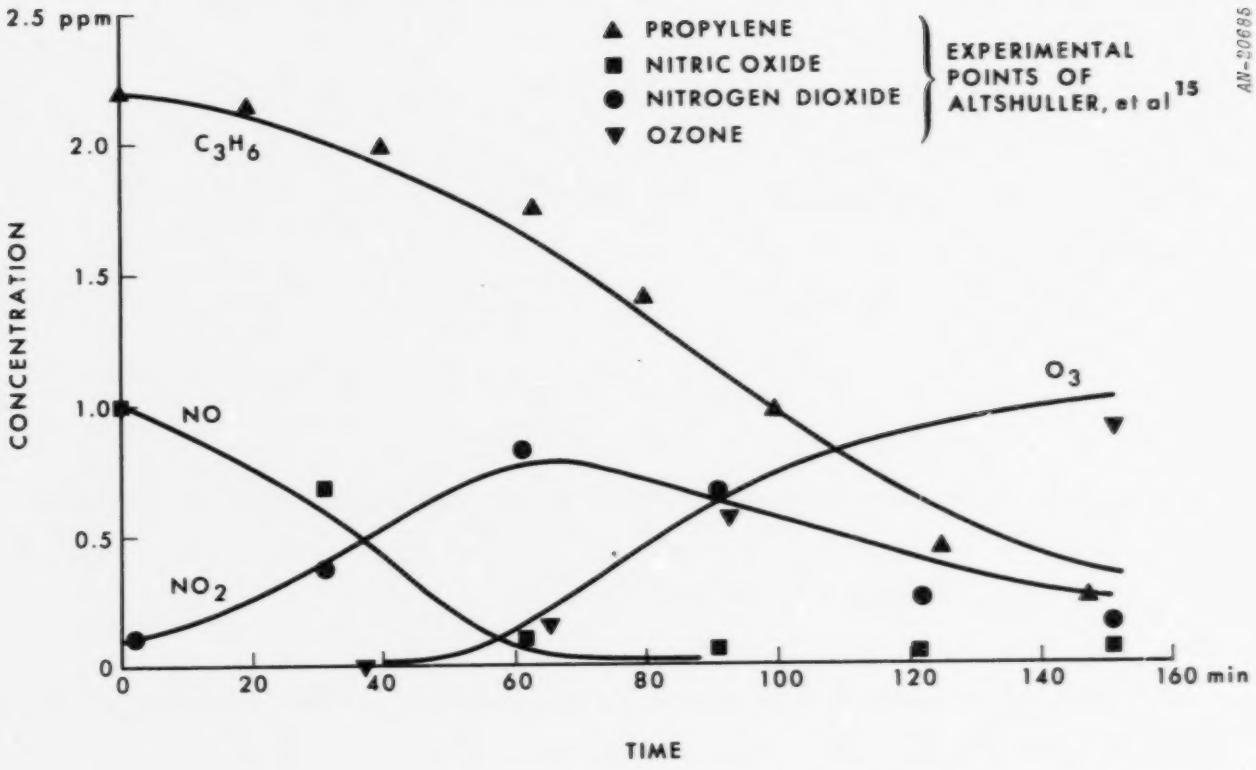

Figure 3. Computed Curves Compared With Experimental Points

TABLE 1

RATE COEFFICIENTS FOR MODEL
HYDROCARBON/NITRIC OXIDE MECHANISM

(Stoichiometry imbalances may occur
because of lumped parameter assumptions.)

Reaction	Model Values From Validation	Nominal Values for Propylene System[14]
$h\nu + NO_2 \rightarrow NO + O$	0.4 min^{-1}	0.4 min^{-1}
$O + O_2 + M \rightarrow O_3 + M$	1.32×10^{-5} $ppm^{-2}min^{-1}$	1.32×10^{-5} $ppm^{-2}min^{-1}$
$O_3 + NO \rightarrow NO_2 + O_2$	40 $ppm^{-1}min^{-1}$	22-44 $ppm^{-1}min^{-1}$
$O + HC \rightarrow 2RO_2$	6100 $ppm^{-1}min^{-1}$	6100 $ppm^{-1}min^{-1}$
$OH + HC \rightarrow 2RO_2$	80 $ppm^{-1}min^{-1}$	244 $ppm^{-1}min^{-1}$
$RO_2 + NO \rightarrow NO_2 + 0.5\ OH$	1500 $ppm^{-1}min^{-1}$	122 $ppm^{-1}min^{-1}$
$RO_2 + NO_2 \rightarrow PAN$	6 $ppm^{-1}min^{-1}$	122 $ppm^{-1}min^{-1}$
$OH + NO \rightarrow HNO_2$*	10 $ppm^{-1}min^{-1}$	99 $ppm^{-1}min^{-1}$
$OH + NO_2 \rightarrow HNO_3$*	30 $ppm^{-1}min^{-1}$	300 $ppm^{-1}min^{-1}$
$O_3 + HC \rightarrow RO_2$	0.0125 $ppm^{-1}min^{-1}$	0.00927 - 0.0125 $ppm^{-1}min^{-1}$
$NO + NO_2 \rightarrow 2HNO_2$**	0.01 $ppm^{-1}min^{-1}$	
$h\nu + HNO_2 \rightarrow NO + OH$	0.001 min^{-1}	

*Rate constant lumps third body concentration

**Water vapor lumped into rate coefficient

B. INFLUENCE OF INITIAL COMPOSITION

1. Synergism Between Hydrocarbons

The fact that free radicals produced in the photooxidation of one hydrocarbon can accelerate the attack on a coexistent hydrocarbon has been illustrated with experimental findings by Altshuller and Bufalini.[16] Because of the limited understanding of detailed interactive mechanisms, we limited our multiple hydrocarbon investigation to a simple parametric study. Using a truncated version of the mechanism in Table 1, we added a parallel series of oxidation steps. This scheme is shown in the flow chart of Fig. 2 with dashed lines along the bottom portion of the diagram.

In the parametric study, the same initial values of total hydrocarbon and nitric oxide as those in Fig. 3 were employed. The hydrocarbon, however, was partitioned into two hypothetical compounds one having triple the (OH + HC) rate constant and the other having one-third the (OH + HC) rate constant as propylene. The compound with the tripled rate is called species "B" and the one with the decreased rate is called species "A". All other reactions in the scheme are the same in all respects as their counterparts in the (C_3H_6 + NO_x)-system.

Figure 4 shows the hydrocarbon decay curves from the parametric study. On the same coordinates we plot curves for model calculations of pure hydrocarbon "A", pure hydrocarbon "B", and pure propylene for comparative purposes with the half-and-half mixture of hypothetical compounds. The most interesting aspect of Fig. 4 is that the mixture decays faster than propylene even though it contains equal quantities of "A" and "B" which bracket propylene symmetrically. The coupling between the two hydrocarbons occurs via the RO_2 conversion of NO to NO_2 and the production of OH . Evidently the combination of the rapid incubation (afforded by the reactive hydrocarbon) with the twofold chain-branching is sufficient to increase the decay rate over that of pure propylene.

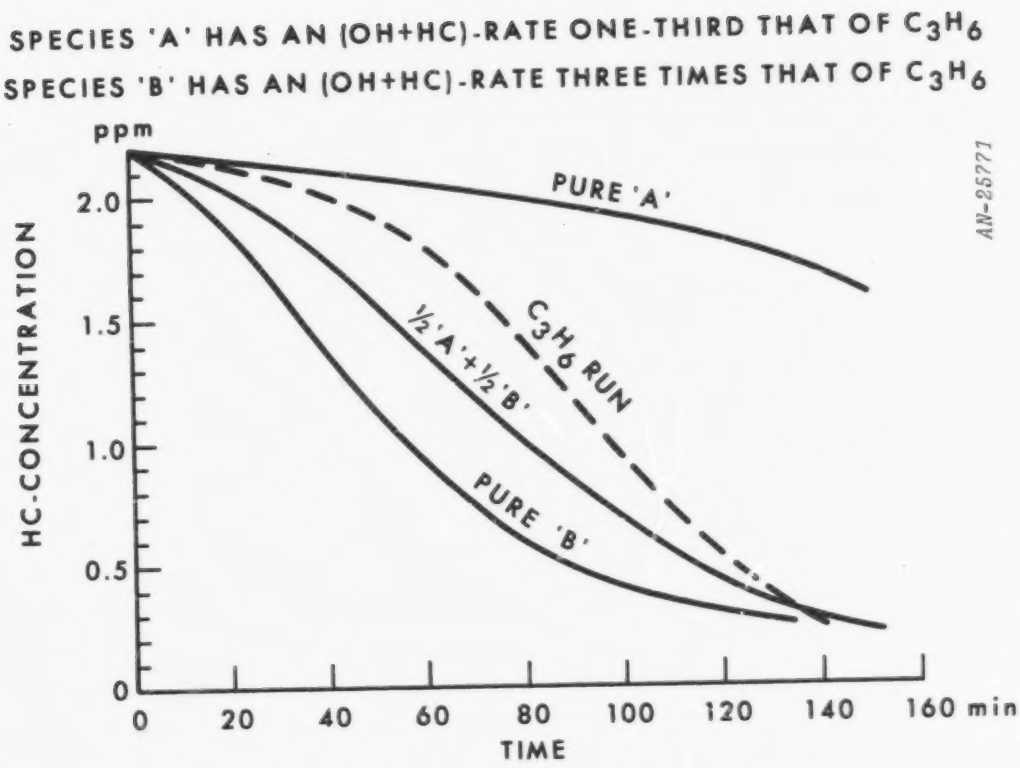

Figure 4. Hydrocarbon Decay With Two Reactivities

Figure 5 shows corresponding curves for ozone buildups predicted in the computer experiment. Again the combination seems to exceed the pure propylene in its rapidity to produce ozone. This occurs because of the enhanced conversion rate of nitric oxide to nitrogen dioxide stimulated by the early abundance of RO_2 generated by the high-reactivity fraction.

These findings illustrate a plausible mechanism for the interaction of multiple hydrocarbons. In future applications of our photochemical/diffusion model this type of representation is likely to be more realistic than a super-detailed single hydrocarbon mechanism with many adjustable constants. Also, other radical interactions like $RO_2 + HC$ and $RCO_3 + HC$ might provide plausible coupling paths[16] in addition to the hydroxyl attack on the hydrocarbon. Indeed, other forms of coupling may favor the slower reacting hydrocarbon in a similar numerical experiment with a half-and-half mixture.

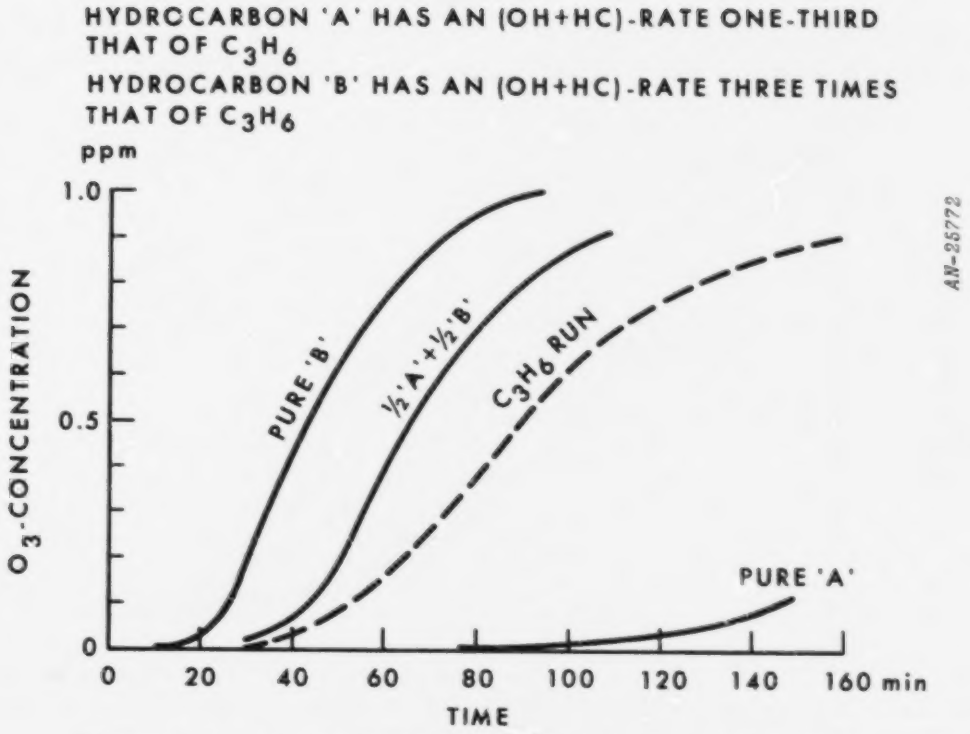

Figure 5. Ozone Buildup With Two Reactivities

2. Modeling the Influence of NO_x/HC-ratio on Oxidant Production

Our main purpose in including the chain termination details for nitrogen oxides in the previous subsection was to improve the modeling of initial mixture effects. It will be recalled that our earlier report[1] issued a caveat restricting the seven-step mechanism to a narrow range of NO_x/HC ratios. Later, Seinfeld[17] pointed out that the slope of the curve of peak oxidant versus NO_x/HC-ratio did not even have the correct sign. If modeling is to be used to evaluate hypothetical abatement strategies, it is clear that this deficiency must be remedied.

Figure 6 shows the results from the twelve-step* mechanism given in Table 1. Experimental results for pure and mixed hydrocarbons are shown on this plot of peak oxidant versus NO_x/HC-ratio. The model mechanism displays a monotonically declining trend of oxidant production as the oxides of nitrogen increase. Both of the pure hydrocarbons

*Stationary state treatment of O-atoms reduces this to eleven.

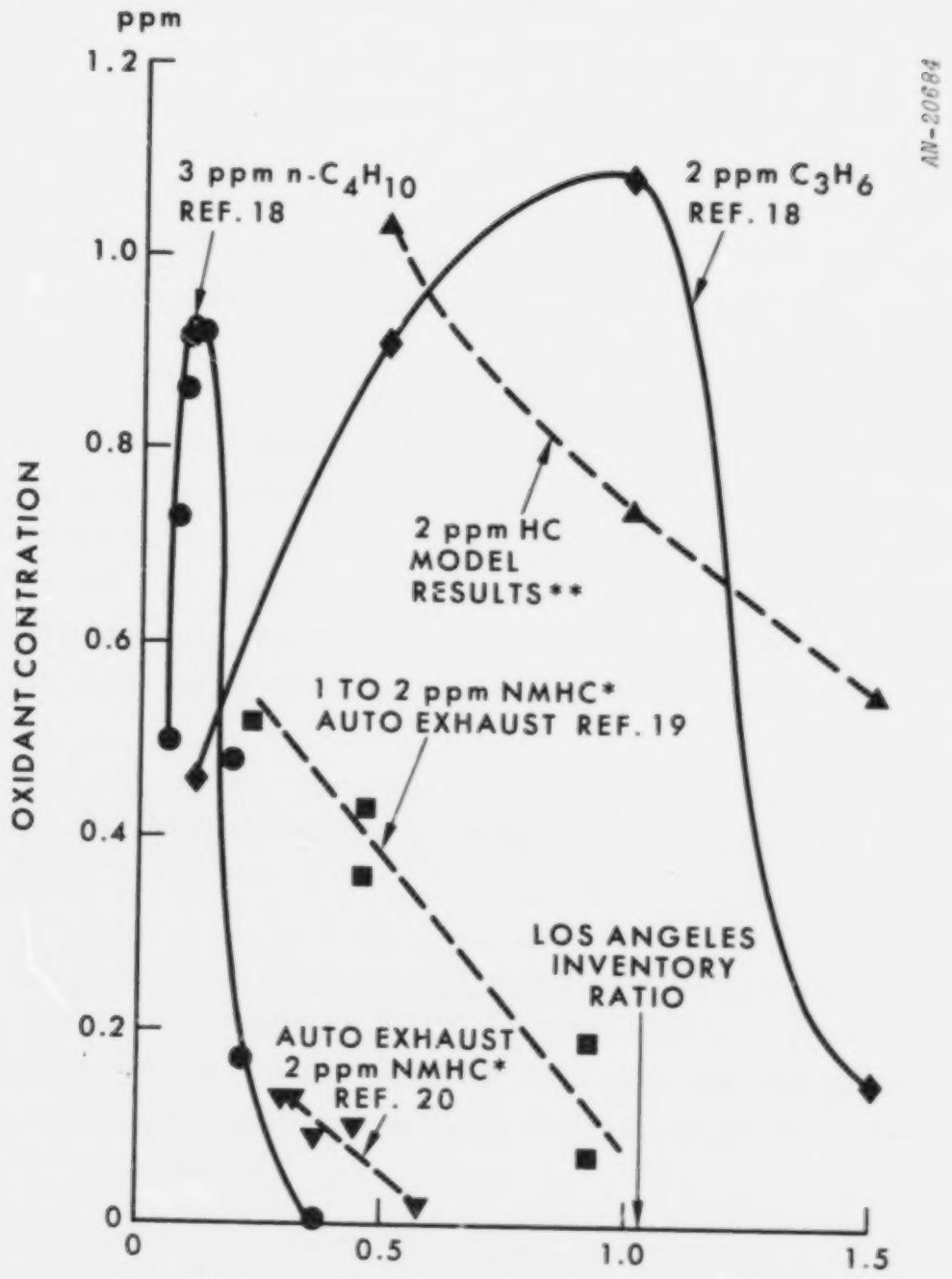

*NMHC:NON-METHANE HYDROCARBON

**THIS CURVE IS LOWERED CONSIDERABLY BY OUR SUBSEQUENT ADOPTION OF ONE-HALF THE PROPYLENE RATES FOR ATMOSPHERIC CALCULATIONS

Figure 6. Influence of NO_x:HC-Ratio on Oxidant Production

measured by Altshuller, et al., show peaks at widely separated values of the mixture ratio. It seems plausible then that the typical mixture of atmospheric pollutant hydrocarbons should show a decrease of oxidant with increasing NO_x/HC-ratio. This is supported by the fact that the relative abundance of hydrocarbon species decreases with increasing reactivity. Now since the low reactivity species peak at lower NO_x/HC-ratios the combined effect should give a negative slope.

The two plots on Fig. 6 of oxidant production from diluted and irradiated automobile exhaust[19,20] both have negative slopes comparable to that of the model. As stated earlier, our purpose in using chamber data for propylene to validate the mechanism is to capture the main features of the experiments that apply to the atmosphere. If, on the other hand, propylene were the subject of our study, we would proceed to expand on the mechanism to get the proper curve shape shown in Fig. 6.

Having subjected the mechanism to these laboratory tests, we use it in its present form for atmospheric validation studies described in a later section.

3. Examination of Carbon Monoxide Effects

Recent work in photochemistry[13,21,22] of smog has suggested that carbon monoxide may play a role in accelerating the photooxidation of hydrocarbon/nitric oxide mixtures. The mechanism suggested is

$$OH + CO \rightarrow CO_2 + H \qquad (14)$$

$$H + O_2 + M \rightarrow HO_2 + M \qquad (15)$$

$$HO_2 + NO \rightarrow OH + NO_2 \qquad (16)$$

$$HO_2 + NO_2 \rightarrow 2HNO_2 \qquad (17)$$

Reaction (15) is postulated to contribute HO_2 rapidly as it responds to the presence of H-atom, and reaction (16) enhances the NO-to-NO_2 conversion already occurring in reaction (6). Likewise, the hydroxyl radical supplied by reaction (16) goes on to react with the hydrocarbon in reaction (4), producing RO_2-radicals in a branched chain already described. Reaction (17) is a chain termination step suggested for HO_2.

The key feature we wish to examine in this alternate path is the competition of CO with hydrocarbon for the hydroxyl radicals. The rate constant for $OH + C_3H_6$ suggested in Ref. 14 is approximately equal to that suggested in Ref. 21 for $OH + CO$. We tried a wide range of (OH + CO)-rates holding the basic system at the values in Table 1. Since reaction (15) is fast, reactions (14) and (15) were added to give the overall reaction

$$O_2 + OH + CO \rightarrow CO_2 + HO_2 \qquad (18)$$

The rate constant for reaction (16) was taken to be the same as its RO_2-analogue, reaction (6), and the rate constant for reaction (17) was assigned the value of 1.2 $ppm^{-1}min^{-1}$ based on the estimate in Ref. 14. The species O_2 is carried implicitly in the calculation, and the rate constant for reaction (18) is varied parametrically for this study.

Beginning with (CO + OH)-values at the level suggested in Ref. 21, ($k_{18} \approx 200$ $ppm^{-1}min^{-1}$) we found very rapid NO-to-NO_2 conversion and HC disappearance with 100 ppm added CO. Only when k_{18} was lowered to 1 or 2 $ppm^{-1}min^{-1}$ did we obtain only small effects. Since much experimental verification is yet to be done, only a limited effort was devoted to this aspect of the study. Table 2 summarizes the main findings. It indicates that the half disappearance time of NO is the strongest effect of k_{18} on the system, and the half-disappearance time of hydrocarbon is least affected. Both the peaking time for NO_2 and the half-rise time of ozone are moderately sensitive to the rate constant.

TABLE 2

INFLUENCE OF 100 ppm CARBON MONOXIDE ON THE SYSTEM SHOWN IN FIG. 3 WITH VARIOUS VALUES OF THE RATIO OF (OH + HC)/(OH + CO) REACTION RATE COEFFICIENTS

k_4/k_{18}	$t_{1/2}$ - NO(min)	t_{pk} - NO_2(min)	$t_{1/2}$ - HC(min)	$t_{1/2}$ - O_3(min)
0.4*	<1	4	40	10
4	6	13	48	22
40	25	43	73	62
80	29	52	81	73
System in Fig. 3 (No CO)	36	66	92	83

*This is with k_{18} set at the estimated value from Ref. 21.

In any event, whether we use the estimated rate of (OH + CO)-reaction or even only preserve its ratio to that of the (OH + HC)-reaction suggested in Ref. 14, we get very large effects. Other work[12] suggests a much larger (OH + HC)-rate constant for propylene. In view of our findings and of the wide disagreements on some of the rates, a very real need exists for definitive experimentation to achieve a deeper understanding of the kinetics.

III. MATHEMATICAL AND METEOROLOGICAL IMPROVEMENTS

Our previous study brought out some of the limitations which hamper the original time-dependent atmospheric model. This model is based on a slab geometry and is solved by a Crank-Nicolson technique.[23] The omission of advection limited the calculation to places and times characterized by stagnant conditions (hence our choice of the October 1968 episode for Huntington Park validation data). Admittedly, this is a case that the plume models (described in Refs. 2, 3, and 4) are incapable of handling, but applications demand that cases with wind transport be treated. Our original response to this need took the form of an Eulerian governing equation for species concentration:

$$\frac{\partial c}{\partial t} + u \frac{\partial c}{\partial x} = \frac{\partial}{\partial z}\left(D \frac{\partial c}{\partial z}\right) + R \qquad (19)$$

where

c = concentration

t = time

x = downwind distance

u = wind speed

z = height above ground

D = diffusion coefficient

R = chemical reaction rate

Solutions of Eq. 19 are costly because of the need to suppress artificial diffusion* by refining mesh and step size. Smog chamber analyses use just the first and last terms in Eq. 19 so that they depend on ordinary differential equations. These are solutions which describe the time-dependent behavior of a homogeneous gas mixture. We used standard Runge-Kutta techniques to solve them in the original code.

---

*Artificial diffusion is an error from numerical differencing of the equation. It produces effects that resemble physical diffusion in the x-direction.

The combined needs for computing efficiency and meteorological realism have been met by improvements described in this section. The first two subsections describe the incorporation of a classical approximation method into our numerical integration. The implementation of these computing techniques strengthen the study by allowing numerous modeling trials on both laboratory and atmospheric cases. The final subsection outlines the change from Eulerian to semi-Lagrangian coordinates in the meteorological formulation. By following air masses we use a natural coordinate system thereby eliminating the artificial diffusion errors.

A. APPLICATION OF PADÉ APPROXIMANTS TO SMOG CHAMBER CALCULATIONS

The chemical model previously described is implemented in rate equations which must be integrated numerically. Because of the widely varying reaction rates, the equations possess a characteristic known as "stiffness" which makes their integration difficult. In the interest of economy and accuracy, special techniques must be employed in obtaining a solution. Below we describe a method which utilizes Padé approximants.[24,25] For these ordinary differential equations, the procedure has yielded significant speed improvements over the Runge-Kutta method previously used.

For this class of problem, the implicit approach is the basic advantage of the new method, thus guaranteeing stability. Consequently accuracy controls step size. This provides the principal gain in computing time.

The rudiments of the integration method are twofold. One involves a linearization of the nonlinear chemical term at every step; the other an approximation of the exponential term that appears as a result of the linearization operation. Thus, consider the following system of equations that describe the changes in species concentration due to chemical reaction:

$$\frac{dc}{dt} = R(c) \tag{20}$$

where c = vector of species concentrations

$R(c)$ = vector of chemical reaction rate functions

$$c = \begin{bmatrix} c_1 \\ c_2 \\ \cdot \\ \cdot \\ \cdot \\ c_s \end{bmatrix} \qquad R(c) = \begin{bmatrix} R_1(c) \\ R_2(c) \\ \cdot \\ \cdot \\ \cdot \\ R_s(c) \end{bmatrix}$$

s = number of chemical species

To linearize the rate vector $R(c)$, we expand it about c_o in a Taylor series. The subscript "o" denotes evaluation at some time $t = t_o$. Thus

$$R(c) = R(c_o) + J(c - c_o) + O(\Delta c)^2 \tag{21}$$

where

$$J = \left[\frac{\partial R_i}{\partial c_j}\right] \qquad i,j = 1, 2, \ldots, s$$

is the matrix of order $(s \times s)$ of first derivatives (the Jacobian matrix) of the rate function. Substituting Eq. 21 into Eq. 20 yields

$$\frac{dc}{dt} = Jc + B \tag{22}$$

where $B = R(c_o) - Jc_o$. It should be noted that at time $t = t_o$ the quantities c_o, $R(c_o)$, and J are known. Hence, the matrix differential

equation (22) is a linear equation with constant coefficients and a constant forcing function. Its formal solution is, therefore,

$$c(t) = e^{J\Delta t}\left[c_o + J^{-1}B\right] - J^{-1}B \tag{23}$$

where J^{-1} denotes the inverse (or reciprocal) of the matrix J.

An approximate solution of Eq. 22 is obtained from Eq. 23 by suitably approximating the matrix exponential $e^{J\Delta t}$. This is accomplished by means of the Padé approximants of the exponential function. These Padé approximants are rational functions of the form

$$e^{J\Delta t} \simeq \frac{P(J\Delta t)}{Q(J\Delta t)} = Q^{-1}P \tag{24}$$

where $P(J\Delta t)$ and $Q(J\Delta t)$ are matrix polynomials of degree p and q, respectively. They are defined by

$$P = \sum_{k=0}^{p} \frac{(p+q-k)!p!}{(p+q)!k!(p-k)!} (J\Delta t)^k \tag{25a}$$

$$Q = \sum_{k=0}^{q} \frac{(p+q-k)!q!}{(p+q)!k!(q-k)!} (-J\Delta t)^k \tag{25b}$$

Thus, substituting Eq. 24 into Eq. 23 we obtain

$$c(t) = Q^{-1}P\left[c_o + J^{-1}B\right] - J^{-1}B \tag{26}$$

The choices $p = q = 1$ and $p = q = 2$ are especially useful. The former yields a third-order integration formula, the latter a fifth-order formula. As an example, for $p = q = 1$ we obtain from Eq. 25:

$$P = I + 1/2\ J\Delta t \qquad \text{and} \qquad Q = I - 1/2\ J\Delta t \tag{27}$$

where I is the identity matrix. Substituting Eq. 27 into Eq. 26 yields, after the appropriate manipulations,

$$c(t) = c_o + [I - 1/2\ J\Delta t]^{-1}\Delta t R(c_o) \tag{28}$$

Equation 28 has a form that is especially well-suited for digital computation. Note that the process requires at every time step: (1) the evaluation of $R(c)$ and J, and (2) the inversion of the matrix Q. The latter is by far the more computationally costly of the two requirements. In our case, the number of species determines the size of the matrix to be inverted. Since this number is not large in our model, the matrix inversion poses no special problems. Fortunately the number of species is usually smaller than the number of reactions.

Table 3 shows examples of the gains obtained using the new computational scheme. The typical real-time/computer-time ratio was increased from 36/1 to 180/1. Perhaps more significant is the fact that the Padé method has allowed us to obtain acceptable solutions in situations where Runge-Kutta either failed to converge or produced spurious solutions. One such instance is the integration of full differential equations for the free-radical species: the Padé method successfully computed solutions without algebraic substitution of stationary-state assumptions whereas Runge-Kutta failed to produce any solution.

As mentioned previously, the step size must still be controlled in order to preserve accuracy. Referring to Eq. 21 we can see that the difference $\Delta c = c - c_o$ determines the order of the truncation error of the linearization operation. The step size must be constrained so that Δc will remain within some bound specified by the user. Our codes contain a variable-step-size feature which ensures that Δc will stay within the prescribed bounds.

TABLE 3

CDC 6400 CENTRAL PROCESSOR TIMES TO RUN
C_3H_6 + NO + hν CHAMBER EXPERIMENT SIMULATION

Type of Run	Runge-Kutta	Padé Approximant
Rapidly changing free radical concentration	2400 seconds	122 seconds
Typical run for 150 minutes real time	250 seconds	50 seconds
Run which diverged for Runge Kutta	267 seconds (diverged at 80 minutes, real time)	50 seconds (ran to completion, 150 minutes real time)

It should also be noted that the nature of our chemical model is such that it leads to a very good first-order approximation as indicated in Eq. 21. This occurs because the full expansion of our particular rate function, R(c) , contains only three terms. Hence in the first-order approximation only one term has been dropped from the expansion.

B. APPLICATION OF PADÉ APPROXIMANTS TO THE ATMOSPHERIC MODEL EQUATION

We now describe the use of Padé techniques to solve the diffusion equation with chemical reactions. The equation in question is referred to a moving air mass. Use of the Lagrangian approach eliminates the second term in Eq. 19 which is reduced to

$$\frac{\partial c}{\partial t} = \frac{\partial}{\partial z}\left(D\,\frac{\partial c}{\partial z}\right) + R(c) \tag{29}$$

where D is the vertical diffusion coefficient and c and R(c) have been defined previously. Applying the "method of lines" to Eq. 29 the partial differential equation is transformed into an ordinary differential equation. Each line represents a different elevation and the resulting ordinary differential equation for a line describes the concentration

changes for a fluid mass moving along the line. The equation for the ith line is derived from Eq. 29 to give

$$\frac{dc_i}{dt} = \frac{D}{(\Delta z)^2}\left[c_{i-1} - 2c_i + c_{i+1}\right] + R_i \tag{30}$$

where $R_i = R(c_i)$, $i = 1, 2, \ldots, M$, where M is the number of mesh points from the ground up to the mixing depth. The symbol c_i defines a vector of s species at the ith point in space. Similarly, R_i defines a vector of s rate functions at the ith mesh point. Thus,

$$c_i = \begin{bmatrix} c_{1i} \\ c_{2i} \\ \cdot \\ \cdot \\ \cdot \\ c_{si} \end{bmatrix}, \qquad R_i = \begin{bmatrix} R_{1i} \\ R_{21} \\ \cdot \\ \cdot \\ \cdot \\ R_{si} \end{bmatrix}$$

In order to solve Eq. 30 by the Padé method, R_i is linearized as in Eq. 21 to yield

$$R_i = R_{io} + J_i(c_i - c_{io}) + O(\Delta c_i)^2 \tag{31}$$

where the zero subscript again denotes evaluation at time $t = t_o$, and J_i is the Jacobian matrix of the rate function at the ith spatial mesh point. Substituting Eq. 31 into Eq. 30 yields

$$\frac{dc_i}{dt} = \lambda\left[c_{i-1} - 2c_i + c_{i+1}\right] + J_i(c_i - c_{io}) + R_{io} \tag{32}$$

where $\lambda = D/(\Delta z)^2$. Writing Eq. 32 more compactly we obtain, after collecting terms,

$$\frac{dC}{dt} = (\lambda A + J)C + R_o - JC_o$$

$$\frac{dC}{dt} = HC + B \qquad (33)$$

where $H = \lambda A + J$, $B = R_o - JC_o$, and

$$C = \begin{bmatrix} c_1 \\ c_2 \\ \cdot \\ \cdot \\ \cdot \\ \cdot \\ c_M \end{bmatrix} \qquad A = \begin{bmatrix} -2I & I & 0 & \cdot & \cdot & \cdot & 0 \\ I & -2I & I & \cdot & \cdot & \cdot & 0 \\ 0 & I & -2I & I & \cdot & \cdot & 0 \\ \cdot & & & & & & \cdot \\ \cdot & & & & & & \cdot \\ \cdot & & & & & & \cdot \\ \cdot & \cdot & \cdot & \cdot & \cdot & I & -2I \end{bmatrix}$$

$$J = \begin{bmatrix} J_1 & & & & \\ & J_2 & & & \\ & & \cdot & & \\ & & & \cdot & \\ & & & & J_M \end{bmatrix} \qquad R_o = \begin{bmatrix} R_{10} \\ R_{20} \\ \cdot \\ \cdot \\ \cdot \\ \cdot \\ R_{MO} \end{bmatrix}$$

Equation 33 now has the same form as Eq. 22 and its formal solution is thus analogous to Eq. 23. Hence

$$C(t) = e^{H\Delta t}\left[C_o + H^{-1}B\right] - H^{-1}B \qquad (34)$$

Approximating the exponential by

$$e^{H\Delta t} \simeq \frac{I + 1/2\ H\Delta t}{I - 1/2\ H\Delta t} = \frac{P}{Q} = Q^{-1}P$$

and substituting in Eq. 34 and simplifying we obtain

$$C = C_o + Q^{-1} G_o \Delta t \tag{35}$$

where

$$G_o = \lambda A C_o + R_o$$

It should be noted that any boundary conditions are implicitly contained in Eq. 35.

Equation 35, which is the analog of Eq. 28, may appear to be simple, but the inversion of Q poses some problems arising from its dimensions. H is an $(M \times M)$ matrix each one of whose entries is an $(s \times s)$ matrix. Hence Q is an $(sM \times sM)$ matrix, and its storage as well as its inversion may be difficult. For example, if we have 10 species ($s = 10$) and 10 space grid points ($M = 10$) then Q is (100×100) and requires rather long computing times as well as large amounts of core storage. However, we take advantage of the structure of Q to develop an algorithm that reduces the problem to the inversion of M matrices of size $(s \times s)$.

It is noted that since J is a diagonal matrix and A is tridiagonal, then H is tridiagonal. Moreover, the off-diagonal entries of H are identity matrices. Forming Q we have

$$Q = I - 1/2\ H\Delta t$$

and it is apparent that Q is tridiagonal, its off-diagonal entries being identity matrices also. Thus only the M diagonal entries of Q need be stored, thereby reducing memory requirements to Ms^2 cells compared to the maximum of $M^2 s^2$. Writing Eq. 35 in the form,

$$QC = QC_o + G_o \Delta t$$

we note that the tridiagonal property of Q allows us to solve for C without explicitly inverting Q. This simplification is afforded by an extended form of Gaussian elimination[23] which requires the inversion of M matrices of size $(s \times s)$. This is preferable to inverting the full $(sM \times sM)$ matrix.

Note that we can also take advantage of the fact that the off-diagonal elements of Q are identity matrices to reduce the amount of computation.

Because series are truncated in these step approximations, some remarks about the resultant errors are necessary. The order of the truncation error of the solution is $O(\Delta t)^3$. This occurs because the approximation of the exponential is

$$e^{H\Delta t} \simeq \frac{I + 1/2\ H\Delta t}{I - 1/2\ H\Delta t}$$

Also, as in the solution of the chemical rate equations, a linearization error of order $O(\Delta C)^2$ appears in the approximate solution. Thus, the same precautions that were taken to preserve accuracy in solving the ordinary chemical rate equations are required in the solution of the atmospheric model equation.

The new scheme has yielded a better than fourfold increase in the real-time/computer-time ratio, i.e., from 7/1 to 30/1.

C. METEOROLOGICAL REFORMULATION OF MODEL

Long computer runs and unacceptable error propagation hampered the operation of the earlier time-dependent advection and kinetics (TADKIN) code.[1] Its application was limited to an analysis of carbon monoxide to examine the influence of advection added to that of vertical diffusion. At the inception of the present work, these severe limitations dictated a reformulation of the advective description before any atmospheric runs

were attempted. Combined with the mathematical advances just described, the semi-Lagrangian embodiment of the diffusion with kinetics (DIFKIN) code extends the application of photochemical diffusion modeling to a great many more cases than previously thought practicable.

Following a center-of-mass fixed coordinate system tied to an air mass, we make use of intrinsic coordinates to avoid artificial diffusion in the horizontal direction. Physical diffusion, therefore, is distinct and identifiable because the moving control volume can be allowed to undergo mass exchange with a neighboring air mass in a prescribed fashion. The question of horizontal spatial resolution is answered by a selection of source grid size and the vertical resolution is set by the choice of the interval size in the z-direction.

Mixing depth or vertical extent of the pollution layer can be handled in one of two ways. In the first, the vertical diffusion coefficient is assigned spatially and temporally dependent values according to the combined effects of shear and buoyancy as turbulent energy sources. The vertical extent of the grid is chosen far above the conventional mixing depth so that the pollutants are automatically confined vertically to a degree which depends on the diffusion coefficient profile. In the second way of specifying the vertical behavior, however, the vertical grid either continuously adjusts to the input values of mixing depth or assumes an average value for the inversion base altitude. We have favored the use of this second approach because it limits the field of computation to the polluted region and thereby conserves computer time. A zero-flux boundary condition is imposed at the top of the net. Vertical diffusion coefficients employed in the earlier work are still used since other reports in the literature appear to corroborate those values.[26,27,28]

The advection patterns are obtained by taking a weighted average of wind-station readings surrounding the point in question. This is truly a receptor-oriented modeling approach since the trajectories are constructed

in hourly upwind segments from the measuring station. Reciprocal distance weighting is employed because of the dominant plane flow pattern which is governed by combinations of sources, sinks, or vortices.* In most cases the three nearest neighbor stations are included in the stepwise upwind tracing or air movement, but occasionally conditions of proximity suggest including only the nearest one or two stations where coastal crossings are involved in the analysis.

Figures 7, 8, 9, and 10 show examples of the paths of air masses estimated in the manner just described. The times of arrival in El Monte are used to identify each trajectory in any subsequent references in this report. The date of September 29, 1969, is chosen because of the rich variety of data that we have available for that day. Note that the earlier morning meandering patterns give way to the dominant onshore flows for all trajectories after 0800 to 0900 hours Pacific Standard Time. The meteorological formulation that we have adopted takes the time and location information from these trajectories to establish the initial conditions and the boundary conditions. Initial conditions are specified as vertical profiles of concentration and boundary conditions as time histories of surface-based pollutant emissions.

Using this approach with data from the two monitoring sites, we are able to match the computing requirements to the data base. Little justification exists at this time to apply complicated grid methods to these validation studies because we only have measurements in great detail from Commerce and El Monte. Just as overly-elaborate chemical models cannot be adequately tested in the atmosphere, neither can highly complex diffusional and atmospheric formulations be checked out with our present store of field observations. Certainly, the day will come when frequent high-resolution readings are made and some of the more detailed theories can be tested.

---

*See Ref. 1 for a discussion of characteristic dimensions.

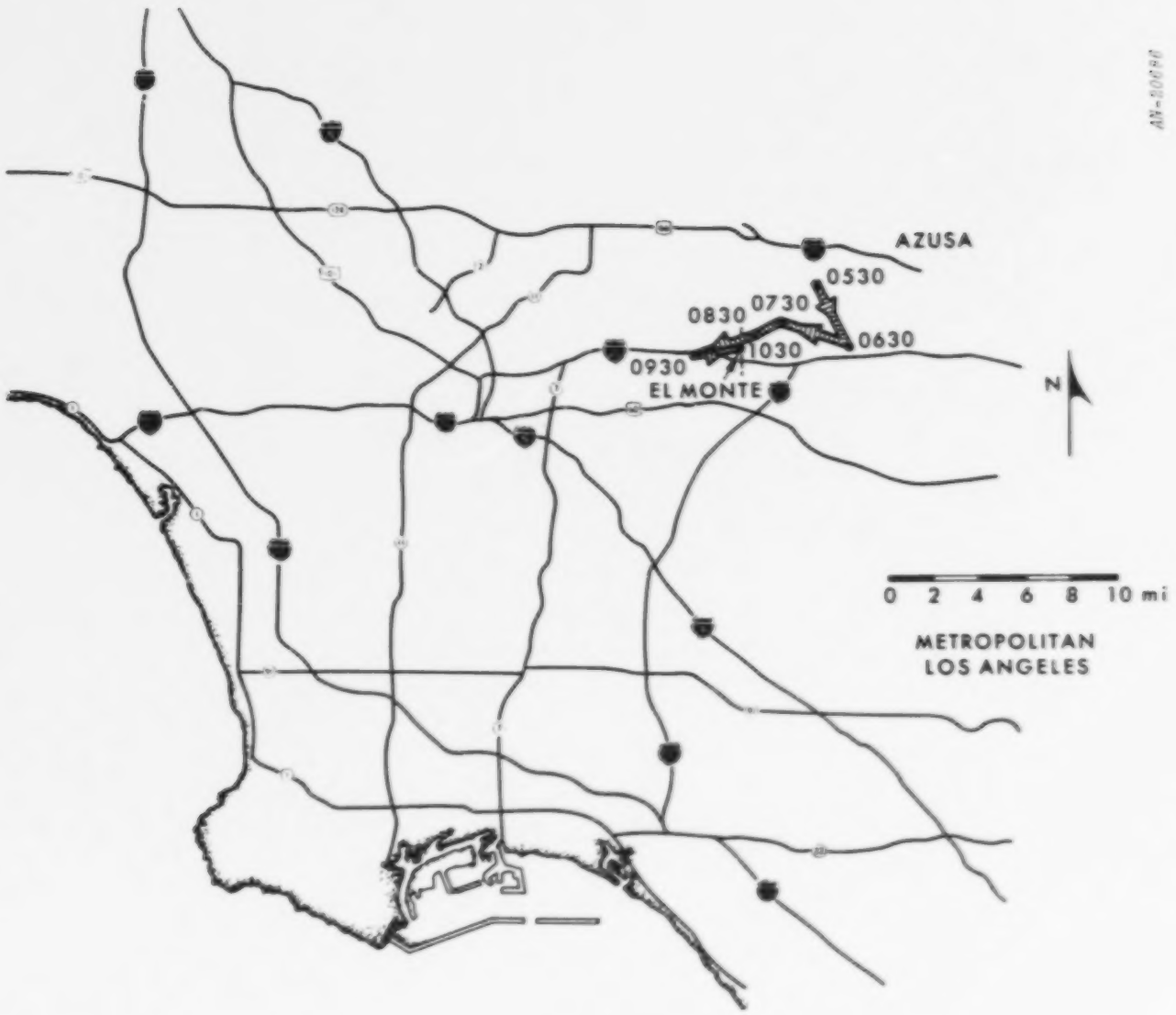

Figure 7. Estimated Trajectory of Air Mass Arriving at El Monte, 1030 hrs, 29 Sept. 1969

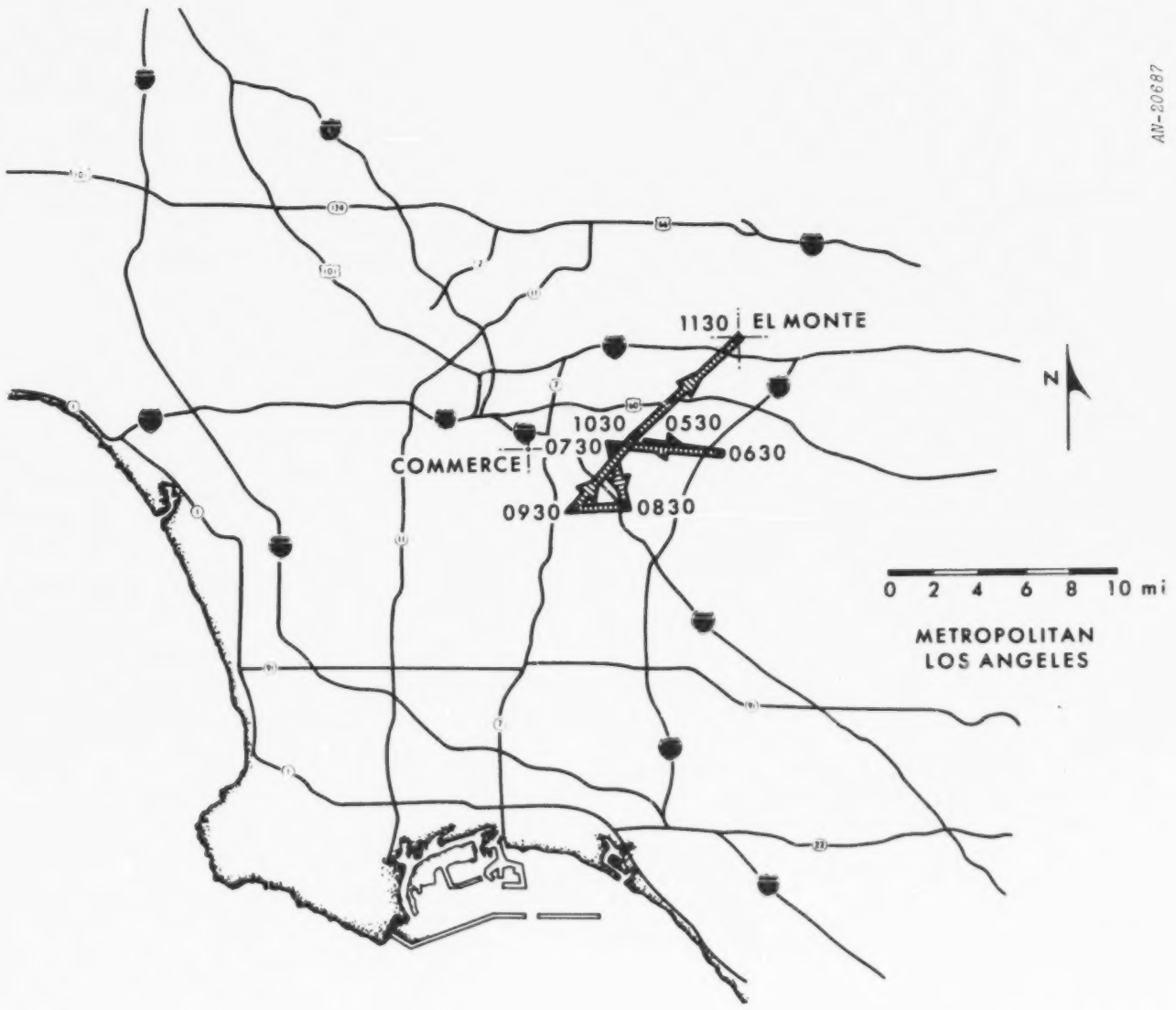

Figure 8. Estimated Trajectory of Air Mass Arriving at El Monte, 1130 hours, 29 Sept. 1969

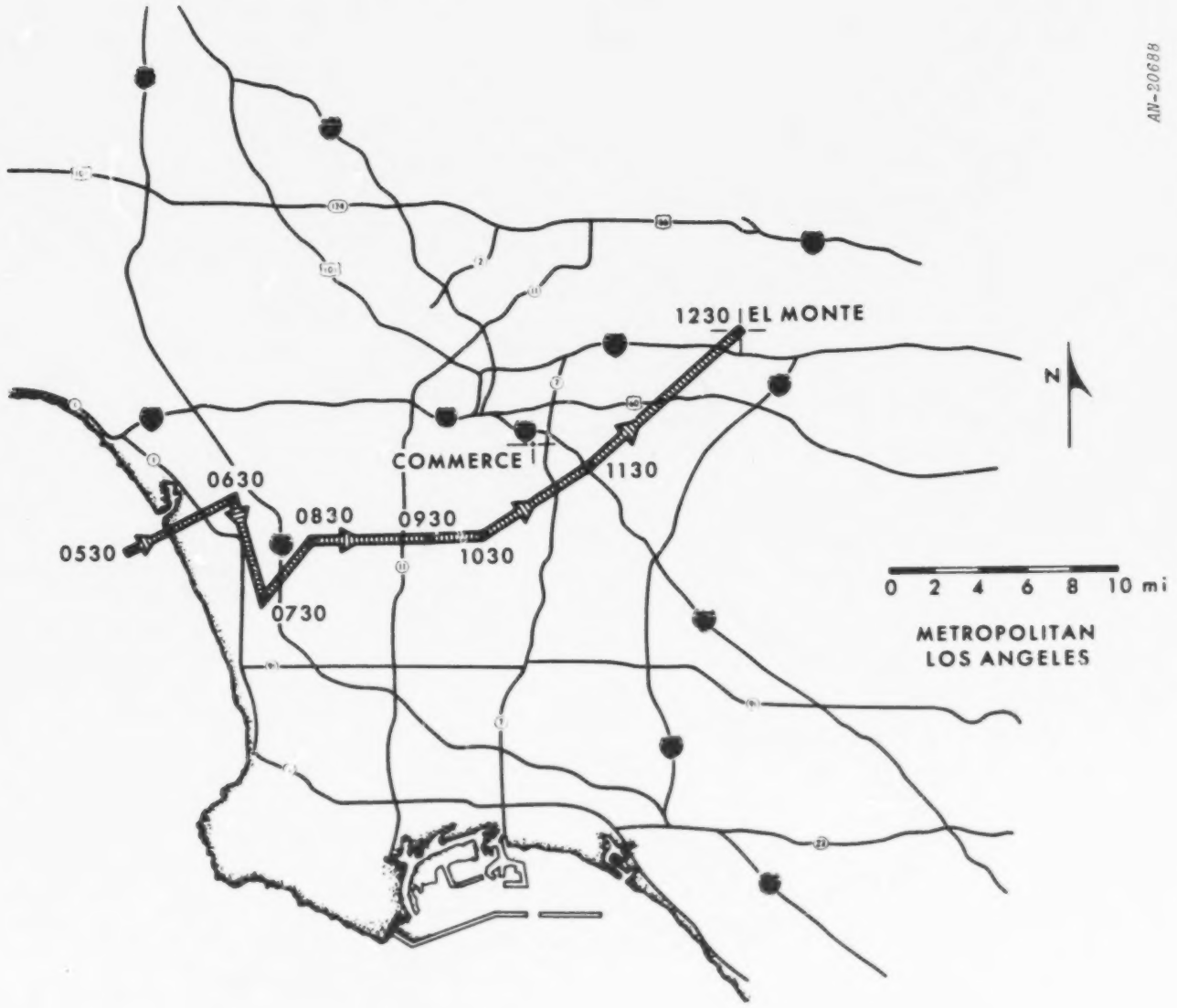

Figure 9. Estimated Trajectory of Air Mass Arriving at El Monte, 1230 hours, 29 Sept. 1969

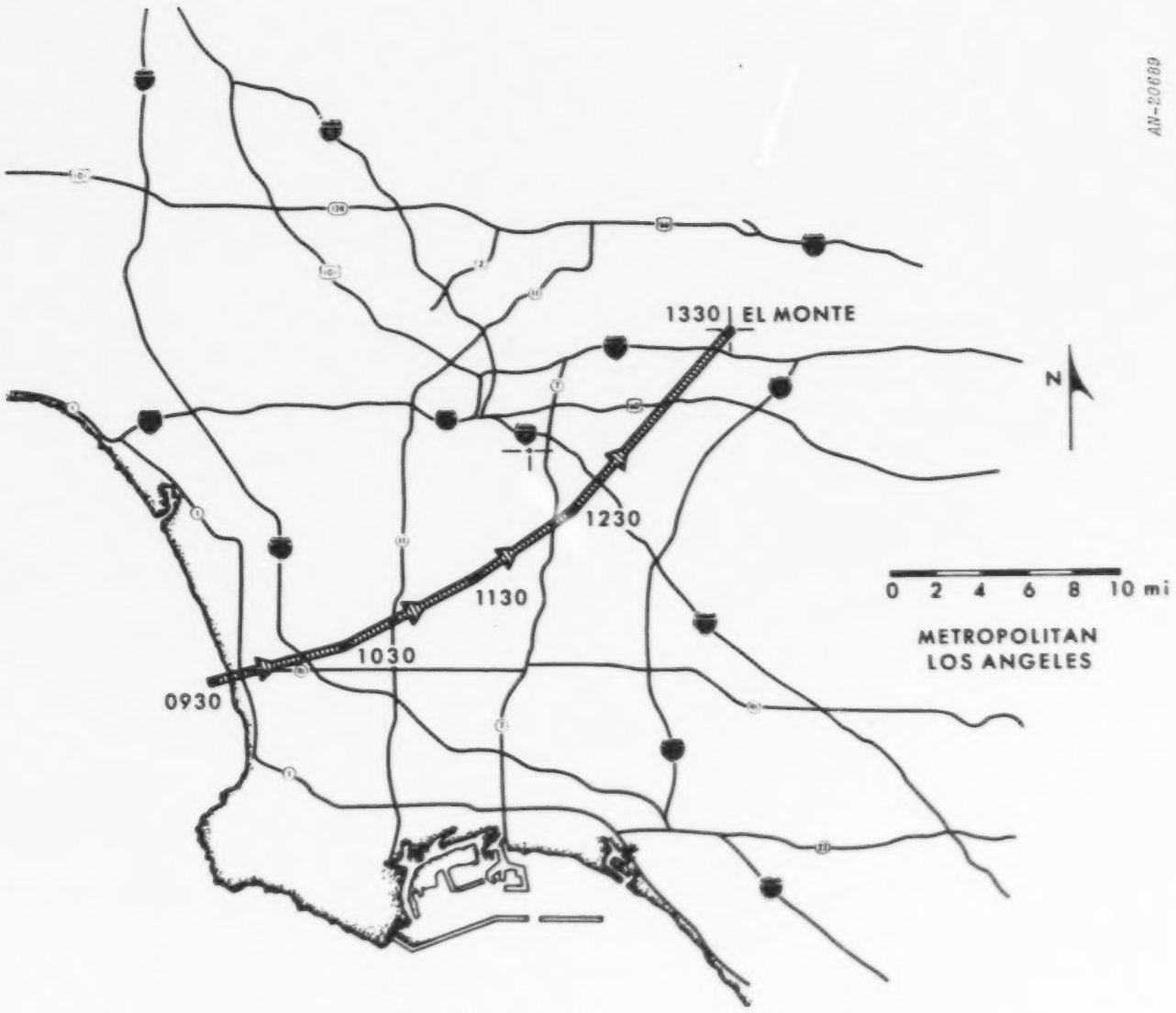

Figure 10. Estimated Trajectory of Air Mass Arriving at El Monte, 1330 hours, 29 Sept. 1969

The next section summarizes our results in testing the improvements we attempted in the chemical, mathematical, and meteorological aspects of the problem. Indeed, many times it appeared that the earlier simple concepts gave better results, but working with better data and more demanding theoretical descriptions than before, we uncovered some significant areas for further investigation.

IV. TESTS OF THE MODEL AGAINST LOS ANGELES BASIN DATA

A. OBJECTIVES OF THE TESTS

With the development of a more complete chemical model than the previous one, the mathematical and meteorological improvements offset the potential computing slowdowns due to added reactions. Having described these advances, we turn now to the task of subjecting the model to tests that are more severe than the previous ones. El Monte is the station of interest in the present work. It is closer to the edge of the urbanized areas than Huntington Park or Commerce, and is, therefore, likely to show larger random fluctuations of pollutant concentrations. In view of the variability of wind directions, this is expected because the air over El Monte may have originated from either high or low pollution areas (see Figs. 7-10). Hence the accuracy of the initial conditions for the test calculation may be as important as the accuracy of the flux boundary conditions.

A primary purpose of this part of the work is to isolate the quality of the model description from possible limitations in the data base. Such limitations can arise either from an insufficient amount or from inaccuracies. We selected September 29, 1969, because it was in an episode of high oxidant levels, and (not coincidentally) the field programs[29] collected a broad sample of airborne as well as ground station measurements. Owing to the prior experience of Scott Research Laboratories, all data were of higher quality than those obtained in 1968. If we can localize the shortcomings of the model (or any that occur in the data) we then possess a guide for action in seeking remedies.

B. REVIEW OF THE PREVIOUS VALIDATION STUDY

A slab treatment of the central Los Angeles basin is the chief distinguishing feature of the previous study.[1] Unlike box models, it accounted for vertical variations of concentration; in fact, a comparison with reactive box modeling demonstrated the need for considering

vertical diffusion. The choice of a centrally located station, Huntington Park, minimized advection effects because the pollution history in surrounding air was not unlike that at the station. Only when considerable ventilation occurs will this break down. To provide added assurances of testing our hypotheses under the assumed conditions, we averaged over a series of relatively stagnant days occurring late in October of 1968.

Figure 11 reviews the results of using our original kinetic model with a conventional Crank-Nicolson diffusion algorithm. This particular plot is for reactive hydrocarbon and it shows dashed lines for the box model results. The symbols f and r refer to the fractions assumed for the nitric oxide flux and the propylene oxidation rate. Experimental results of C_2H_2/NO_x-ratios suggested as much as a fourfold deficit in the NO_x-balance; therefore, we set $f = 1/4$. The aggregate of the hydrocarbon reactivity was one-third to one-half that of C_3H_6, so that $r = 1/2$

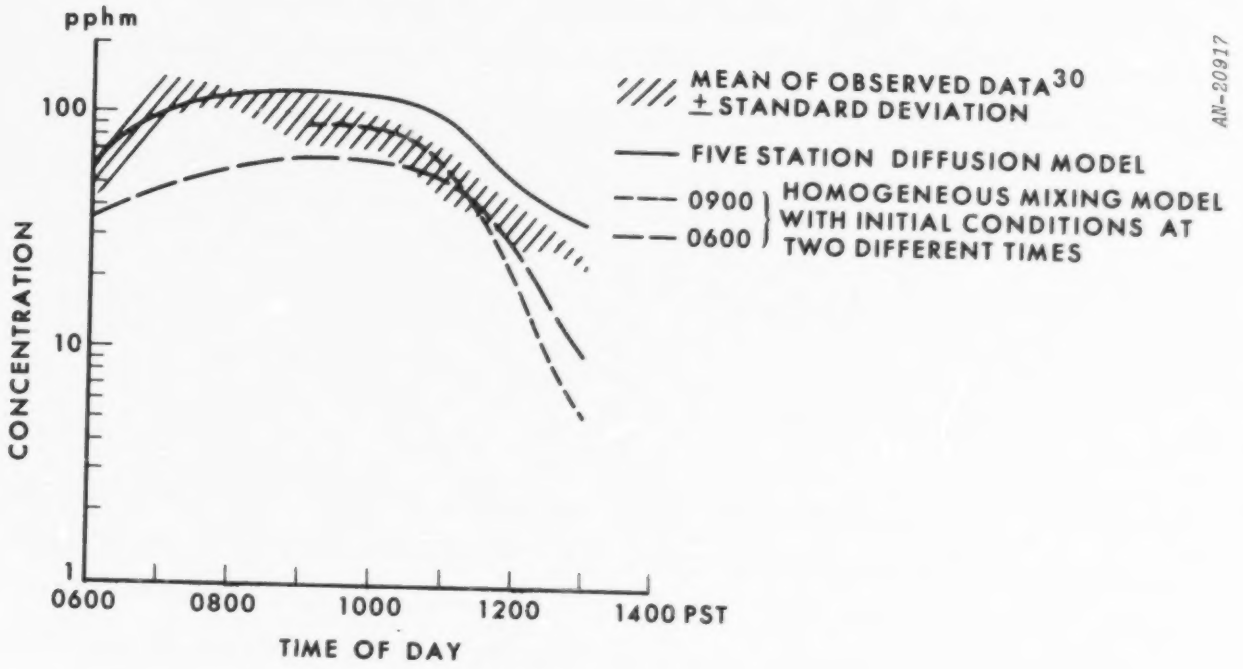

Figure 11. High Reactivity Hydrocarbon Concentration at Huntington Park on Type 2 Days, 1968. f = 1/4; r = 1/2

was employed.* Note that the diffusion model is preferable to the box model, but that advection is inadequately represented in the mid to late morning hours.

Figure 12 shows the oxidant buildup at Huntington Park for the late October 1968 smog episode. Again it is seen that the finite difference diffusion model is superior to the box model. The solid curve representing a solution using a five-station vertical mesh gives nearly the correct peak height and time.

C. SENSITIVITY STUDIES ON 1969 TRAJECTORIES WITH THE EXPANDED MODEL

Based on the semi-Lagrangian formulation of the photochemical/diffusion model, the computed end-point composition of the air masses depends on initial conditions, flux from the ground along the trajectories, and on reaction rates. For our tests, we concentrate on El Monte data because much of the polluted air there comes from somewhere else. This is believed to be a more severe test of the model than that at Huntington Park. The initial conditions are based on measurements insofar as possible. The principal initial values for the 1030 trajectory are as follows for 0730 hours (PST).

c_{HC} = 51 pphm (6 ppm C total HC)

c_{NO_2} = 24.5 pphm

c_{NO} = 3.5 pphm

These were interpolated from the Azusa station data[31] from the Los Angeles County Air Pollution Control District. Reference to Fig. 7 shows the basis of this choice. The reactive hydrocarbon value is derived from the assumptions of 34 percent reactive fraction and an average carbon number of 4 for the reactive family of compounds. These are seasonal averages

*Propylene was used for the baseline validations of smog chamber results.

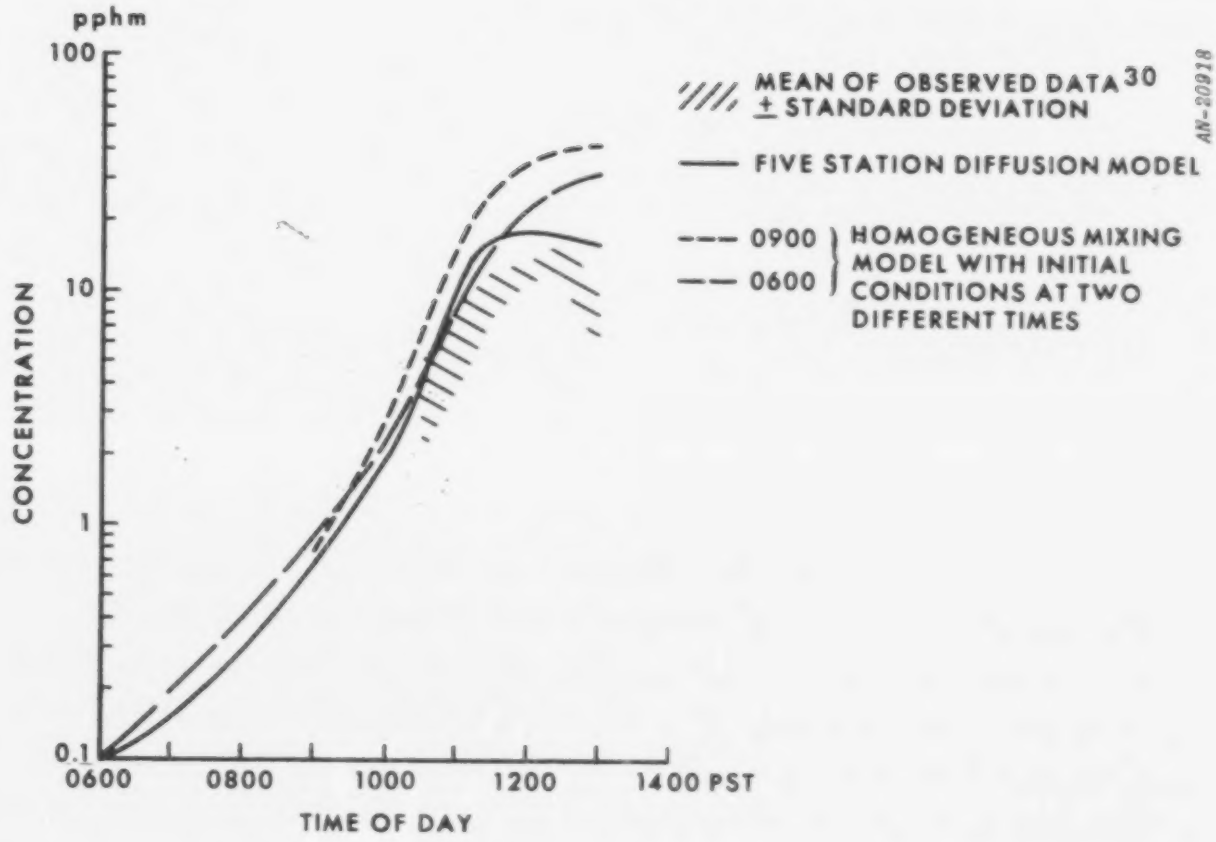

Figure 12. Ozone Concentration at Huntington Park on Type 2 Days, 1968. f = 1/4; r = 1/2

over the 1969 measurement months[29] at El Monte. The analysis that generated the values from gas chromatographic data is discussed elsewhere.[32] Similarly the 0730 initial values for the 1130 trajectory are obtained from the Commerce data log.[29] They are:

$$c_{HC} = 94.5 \text{ pphm } (9.7 \text{ ppm C})$$

$$c_{NO} = 43.9 \text{ pphm}$$

$$c_{NO_2} = 17.4 \text{ pphm}$$

The hydrocarbon conversion factors here are 41 percent reactive fraction and an average carbon number of 4.2.

Since the 1230 trajectory begins near the coast, we employ station 76 (La Cienega Boulevard) measurements for 0630 hours (PST) initial values of nitrogen oxides. No hydrocarbon data are available from that station and an HC/NO_x-ratio of 2 was chosen. Although this is not representative of the inventory ratio, it is representative of many morning air samples. Such an observation further reinforces the suspicion of an NO_x-deficiency on high oxidant days.[32] Thus, the values are:

$$c_{HC} = 54 \text{ pphm}$$

$$c_{NO} = 18 \text{ pphm}$$

$$c_{NO_2} = 9 \text{ pphm}$$

The location of the 1330 trajectory origin is near no station and the data indicate that the initial pollution cannot be neglected. Consequently, results were not obtained for the 1330 trajectory.

For boundary conditions we followed nearly the same procedure as before.[1] The fluxes of reactive hydrocarbon and nitric oxide were obtained by superimposing a source grid on Figs. 7 through 10. The stationary sources were distributed as in the previous work, but updated information was utilized for the vehicular fluxes as they are disposed in space and time. We are especially grateful to Dr. Philip M. Roth, Director of Environmental Studies, Systems Applications, Inc., for providing these data that his organization developed under the sponsorship of the Air Pollution Control Office. Our own emission factors were applied using averages weighted by the vehicle age distribution as described elsewhere.[33] Ultraviolet data from Ref. 29 were employed to get photodissociation rates for NO_2 by means of calibration functions developed in the data analysis study.[32] Inversion base altitudes were averaged from the airborne temperature measurements provided by Scott Research Laboratories.[29]

To examine parametrically the influence of inventory levels, we altered the rate of emissions calculated for ground level. Halving the nominal NO-fluxes is suggested by the departures of the CO/NO_x-ratios and the C_2H_2/NO_x-ratios obtained for high oxidant days.[32] Subsequent halving of both reactive hydrocarbon and nitric oxide fluxes brings us down to the adjustment represented by $f = 1/4$ in Figs. 11 and 12 but preserves the HC/NO_x-ratio. In both cases the full propylene oxidation rates were employed.

Table 4 summarizes the results for trajectory end points. Advancing down the table we note an ever-growing sensitivity of the results to the flux adjustments. This occurs because the increasing wind speed lengthens the trajectories and there is larger relative exposure of the air mass to high pollutant fluxes.

TABLE 4

RESULTS OF MODEL SENSITIVITY STUDY
USING 1969 EL MONTE DATA

Concentrations at El Monte in pphm

El Monte Trajectory Arrival Time (PST)	NO			HC			NO_2			O_3		
	Measured Values	$(1/2)\phi_{NO}$ Full ϕ_{HC}	$(1/4)\phi_{NO}$ $(1/2)\phi_{HC}$	Measured Values	$(1/2)\phi_{NO}$ Full ϕ_{HC}	$(1/4)\phi_{NO}$ $(1/2)\phi_{HC}$	Measured Values	$(1/2)\phi_{NO}$ Full ϕ_{HC}	$(1/4)\phi_{NO}$ $(1/2)\phi_{HC}$	Measured Values	$(1/2)\phi_{NO}$ Full ϕ_{HC}	$(1/4)\phi_{NO}$ $(1/2)\phi_{HC}$
1030	3.4	0.5	0.3	43	34.3	24	16.4	20.5	14.5	13.4	32.6	35.3
1130	3.2	1.5	1.5	64	87.4	70.1	21.3	58.5	48.6	23.6	28.4	24.2
1230	1.5	1.1	1.0	38	67.5	48.1	10.3	49.2	34.6	24.5	30.9	24.8

NOTE: Nominal values of emission fluxes are denoted by ϕ. Hence, $(1/2)\phi$ means that we halved the fluxes derived from inventories.

In the 1030 case, both hydrocarbon and nitric oxide are low, but NO_2 and ozone are high. Changes in the fluxes have marked effects on everything but the ozone. Comparing these end-point compositions with the initial values cited above, we note a strong dependence on initial conditions accuracy for this short time scale. Fortunately the Azusa data are available as an aid in this respect.

For the 1130 results, the ozone and nitric oxide come in closer to the data but NO_2 is extremely high. This is symptomatic of the large departures from the radiation-supported quasi-equilibrium that we noted in analyzing the El Monte data.[32] Although the model does not assume quasi-equilibrium among the three reactions

$$h\nu + NO_2 \rightarrow NO + O$$

$$O + O_2 + M \rightarrow O_3 + M$$

$$O_3 + NO \rightarrow NO_2 + O_2$$

the differential equation solutions nearly always approximate it rather well.

Again, with the 1230 trajectory the ozone and nitric oxide levels match observations reasonably well, but hydrocarbon and NO_2 are both high. Despite the passage of this air from the seashore and then over extensive regions of the central basin, we note that the initial values of the primary pollutants still influence the final concentrations in a dominant manner.

D. HISTORY ANALYSIS OF THE 1030 EL MONTE TRAJECTORY

Because of the relative completeness of initial conditions that we can relate to the Azusa station, we have chosen the 1030 trajectory to discuss in some detail. Examining Table 4 we note an overabundance of ozone at 1030 and a correspondingly rapid completion of $NO \rightarrow NO_2$ conversion. Reactivity analyses[32] and previous modeling studies[1] suggest reduction of the oxidation rate constants. To achieve some level of comparative assessment with the previous work we assign one fourth the nominal NO flux and one half the oxidation rate; hence, $f = 1/4$ and $r = 1/2$ describe the conditions as before. This time, however, we preserve the HC/NO_x-ratio as in the entries in Table 4 and reduce hydrocarbon fluxes by a factor of 2. This means that the difference in end-point concentrations between this case and the $1/4\phi_{NO}$, $1/2\phi_{HC}$ entries is solely due to the rate constant reduction. This differs from the earlier work in which hydrocarbon fluxes were not reduced.

Figure 13 shows the reactive hydrocarbon history starting at Azusa at 0730 and ending at El Monte at 1030 on September 29, 1969. Despite the sharp reduction in hydrocarbon fluxes, the calculated curve stays above the Azusa levels until 1000 hours when it begins to slope-off in the observed manner. The model output clearly bears a closer relationship to the Azusa measurements than it does to the El Monte observations. This problem is typical of the difficulties we encountered in attempting to model conditions at the eastern portion of the basin at El Monte.

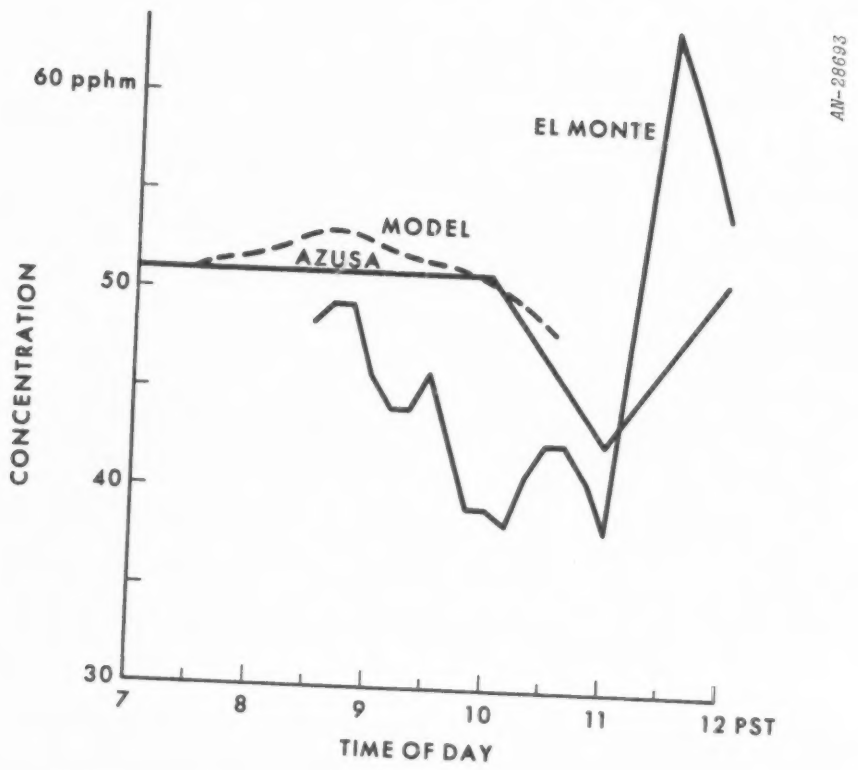

Figure 13. Reactive Hydrocarbon History Along the 1030 Trajectory. f = 1/4; r = 1/2 (Ground level concentrations)

On Fig. 14 we note a sharp drop from the interpolated NO-level between 0730 and 0740 hours. This is reflective of the previously noted failure of the data to approach quasi-equilibrium between NO, NO_2, O_3, and sunlight intensity under high oxidant conditions. The NO-conversion seems to proceed at roughly the observed rate after the transient is absorbed in the system; however, the level ends up closer to Azusa values than to El Monte values. Note that if we were to employ 0830 El Monte concentrations as initial values, we would have a lower HC/NO-ratio and could expect still slower nitric oxide conversion rates. Thus, both nitric oxide and hydrocarbon decay more like the Azusa data than the El Monte data.

The NO_2 behavior on Fig. 15 exhibits more nearly what one would expect than do either the reactive HC or the NO. Proceeding from the end of its transient adjustment to observed sunlight intensity,

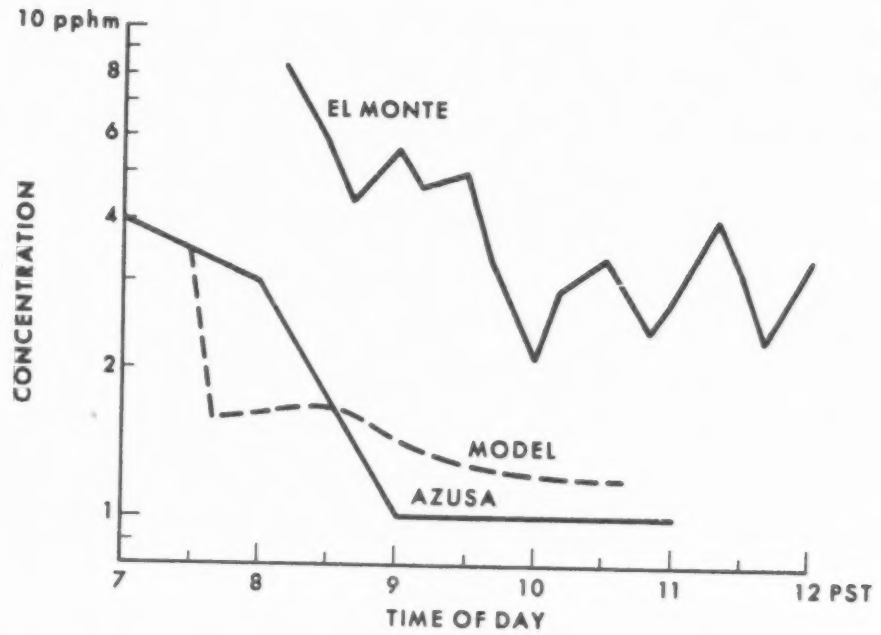

Figure 14. Nitric Oxide History Along the 1030 Trajectory. f = 1/4; r = 1/2 (Ground level concentrations)

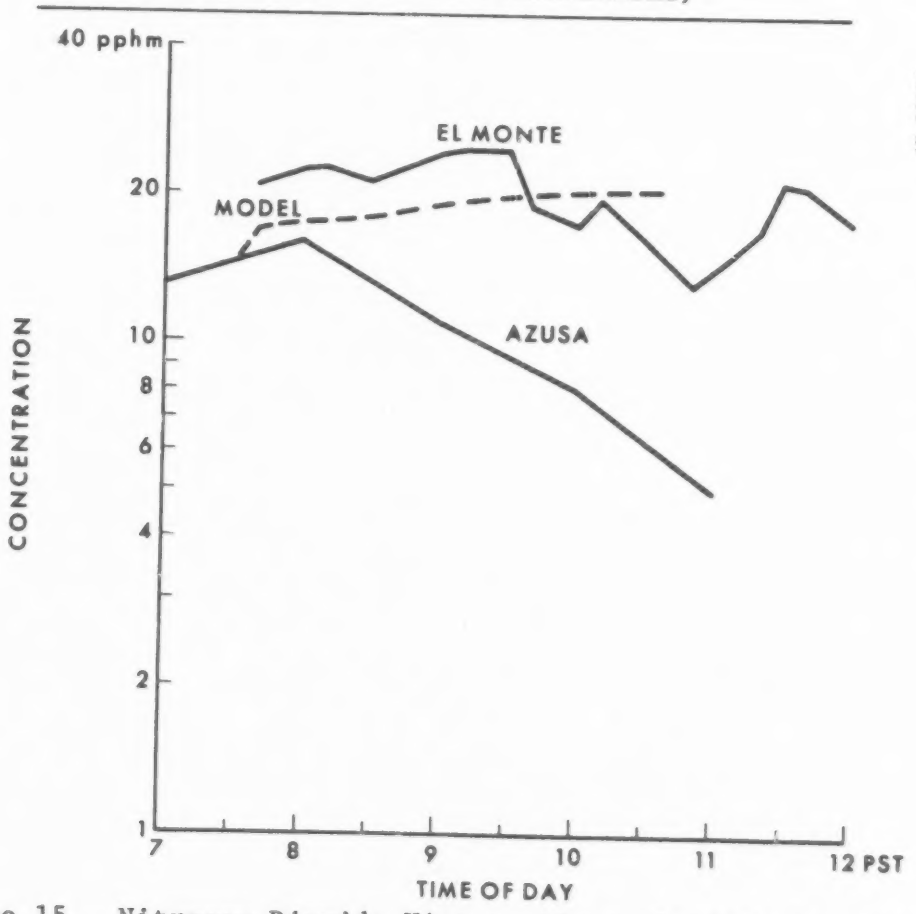

Figure 15. Nitrogen Dioxide History Along the 1030 Trajectory. f = 1/4; r = 1/2 (Ground level concentrations)

the air mass gradually undergoes NO_2-transition from Azusa levels to El Monte levels as it meanders about in the northeastern area of the basin. Nitric oxide conversion supported by increasing sunlight intensities drives the NO_2 upward. The ground-based sources continue to feed in NO as it reacts and diffuses upward.

Summing over NO and NO_2, we get excellent total balance behavior for these oxides of nitrogen. Figure 16 indicates that not only slopes, but also magnitudes are represented rather well in the gradual change of composition moving from initial to final conditions over the three-hour period. Apparently the dominant effect of the good behavior of the NO_2 brings the balance into favorable agreement with the data. It will be recalled that this was a key test in the original choice of $f = 1/4$ after conducting our original modeling study.[1]

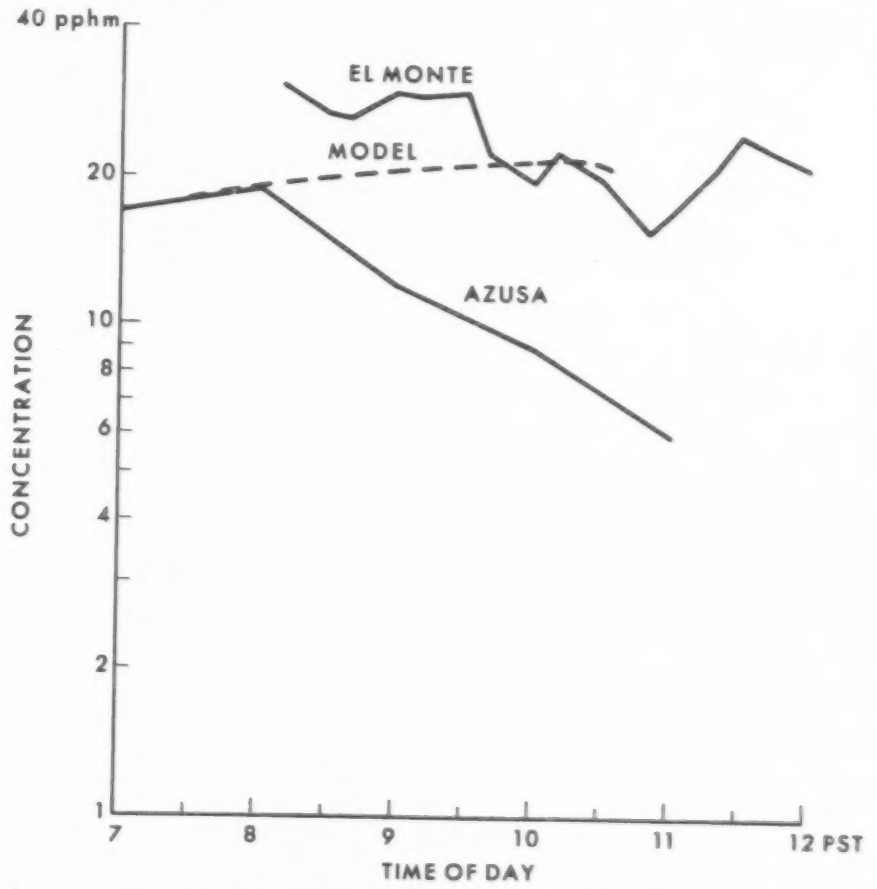

Figure 16. Oxides of Nitrogen ($NO + NO_2$) History Along the 1030 Trajectory. $f = 1/4$; $r = 1/2$ (Ground level concentrations)

Finally, the history of ozone concentration may be seen on Fig. 17. The measurements at both Azusa and El Monte show a remarkable degree of smoothness and regularity compared with the jagged curves of the species displayed in the previous figures. Again, due to the rapid transient response of the $O_3/NO/NO_2$-system to the sunlight ultraviolet intensity, there is a sharp change in the first ten minutes of the model curve. As in the case of NO_2 , however, the ozone undergoes a smooth transition from its origin to its destination. Considering the usual sensitivity of ozone to competing rate determining factors, this degree of realism is gratifying.

If we applied this same set of assumptions to the other trajectories, we would get too little ozone at the end points. Table 4 indicates fair agreement with $f = 1/4$ and $r = 1$ as shown in one of the columns. The hydrocarbon agreement for these other cases would be even worse than it stands if r were decreased to 1/2. Because of low confidence in the initial values that apparently dominate, the other trajectories would likely be less than satisfactory as tests of the model.

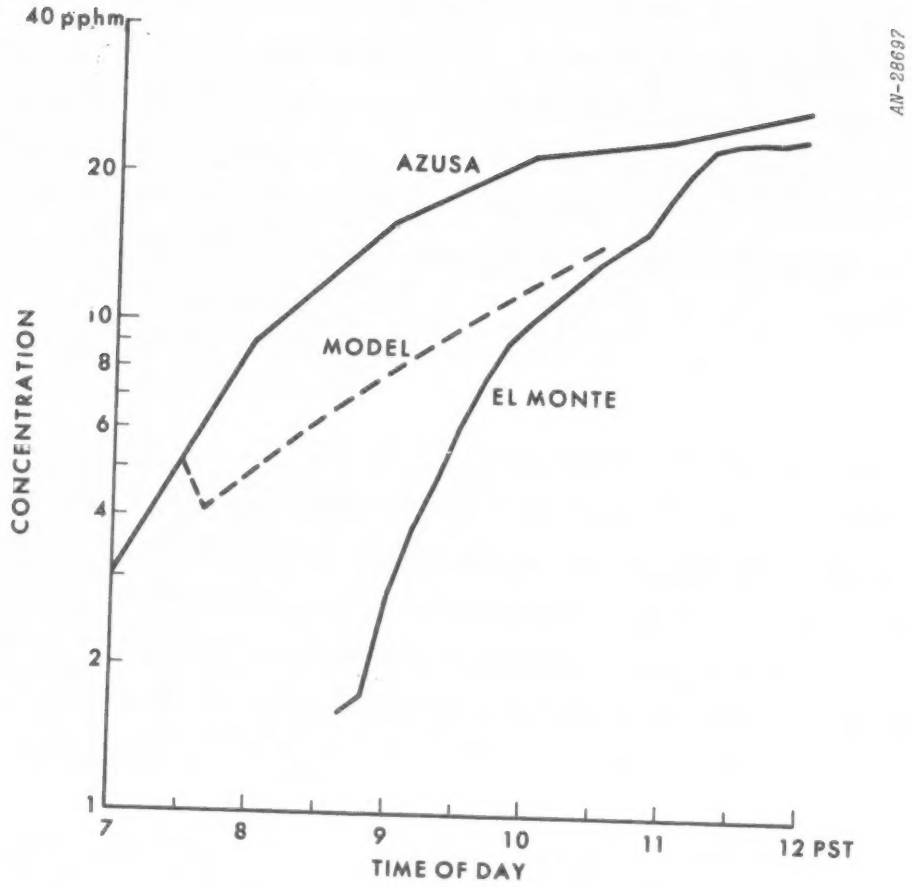

Figure 17. Ozone History Along the 1030 Trajectory. f = 1/4; r = 1/2 (Ground level concentrations)

V. CONCLUDING REMARKS

An overview of these further developments of the GRC photochemical/diffusion model holds answers to many questions and points the way to future research needs. Before detailing the accomplishments and recommending new directions, we might make the general observation that applying and adapting the modeling tools that we possess now appears preferable to initiating effort on far more detailed chemical dispersion formulations. We have maintained a balanced posture in which the model advances and the improvements in measurements have kept pace with one another.

The chemical descriptions offered here hold the main features of the NO_x-chain termination that controls composition effects on secondary pollutant production. In concert with this, the addition of hydroxyl radical chemistry is a first step in explaining the "excess rate" of hydrocarbon oxidation (over that attributable to O-atom attack). Probably one of the most uncertain aspects of the system is our inclusion of HONO formation (from $NO + NO_2$) and opposed by photodissociation. If this is an important feature of the free radical balance, we really need to know the photodissociation absorption coefficients for HONO as well as some of the radical-molecule collisional reaction rates. In his task force report[34] for Project Clean Air, H. S. Johnston stresses the need to consider nitrous and nitric acids in the photochemical mechanism. This suggests a very real need to monitor these compounds in the laboratory experiments and in the atmosphere. Their involvement in aerosols and surface reactions may well hold the key to the apparent anomalies in the nitrogen balance. The identification of chemo-mutagenic effects of HONO is yet another reason that it should be investigated. The brief examination of hydrocarbon synergism shows at least one way that the radical chains are cross-linked to influence combined reaction rates. Experimental data on mixed hydrocarbons will help sort out the most likely mechanisms. Likewise, our small study on possible CO-interference indicates that suggested values of these rate constants indicate a very strong influence on the propylene/nitric oxide system at concentration

levels as high as 100 ppm. It may be that atmospheric hydrocarbons that are not involved in the OH-cycle are far less affected. In any event atmospheric levels of CO are much lower than 100 ppm except in the vicinity of traffic arteries.

Reacting to the need for extended chemical representations, we have applied Padé approximant techniques to the numerical integration algorithms. Speed increases of at least four or fivefold are obtained in the computation comparing the Padé method for the more complex chemical system with previous methods for the simpler system. For equal-sized chemical matrices the improvements would most likely be even better. In the interest of making these advances available to the community at large we show the mathematical steps in some detail.

Besides the mathematical improvements, the atmospheric model has been adapted to a semi-Lagrangian formulation. By following selected air masses we avoid commitments of large quantities of memory and the incursions of artificial diffusion errors. Most important, we do not end up with stacks of computer printout that relate to regions where there are no measurements. It should be added that predictive calculations will become ever more useful, but our present levels of resources and sophistication demand that effort be concentrated on validation. Only in this way can the confidence be built that is needed for applying modeling techniques to implementation planning.

Validation tests of the model for 1969 Los Angeles basin data turned up several useful findings. For time intervals within a diurnal scale, we must use extreme care in selecting initial conditions. A way to overcome this need is to compute for several days of real time on a continuous basis. Increasing the time scale makes sense because episodes tend to cycle through several days. The cost in computing will go up more than proportionately, however, because as time scales increase so must the spatial domain. Perhaps 100 kilometers of urban/rural influence

zone might be needed in lateral expansion. Correspondingly, a larger vertical field will have to be included to account for slow transport within the inversion layer, if there is one. Models that require artificial image flows above the marine layer or that assume artificially inflated "background" levels at the edge of the net will no longer be useful. What used to be boundaries will now be included in the computational field.

The sensitivity tests in the validation studies confirmed some of the suspicions that we expressed earlier;[32] namely, that the quasi-equilibrium relationship between ozone and the oxides of nitrogen does not seem to be recovered in the data. The largest departures are for the highest ozone levels. Attempting to represent the physical setting in a consistent manner, we find it difficult to use the measured ultraviolet intensity to account for the observed ozone buildup and NO-conversion simultaneously. The inconsistency even appears in the initial behavior of a modeling run as a transient "induction" process that rapidly adjusts concentrations to satisfy the rate equations. Unlike some models, ours does not impose the quasi-equilibrium, but rather solves for time history of species with O-atom, RO_2-radicals, and OH in the stationary state.

Because of the extreme dependence on initial conditions, our history analysis concentrates on an air mass with relatively well-defined concentrations at the beginning and the end of its travel. Giving it the initial values we see the concentrations unfold as the air parcel moves through the computed simulation procedure. In view of the sensitivities discovered, the transition of oxidant species O_3 and NO_2 proceeds better than one might expect. The previously adopted biases on the NO-flux and the propylene oxidation rates were confirmed in this run having very different conditions than those in Huntington Park represented by 1968 data.

Much more work remains to be done. We have so many uncertainties in both the data and the model assumptions, that systematic tests must be devised to isolate the individual influences of the various parameters. Our very limited sensitivity study illuminates some of these very serious questions that need to be answered. The anomalous pattern of NO-flux followed from our original work, through the data analysis project, and into this work. Either some very serious deficiency exists in the transport formulation or there are some rapid loss mechanisms for oxides of nitrogen that reduce the apparent emission strengths. In view of the extensive efforts directed toward NO_x-controls high priority must be given to measuring the terms of the nitrogen balance equation in an urban area. Nitric acid vapor, nitrous acid vapors, and particulate nitrates could hold the key to this question. The modeling is not precise enough to pin down the deficit, but the CO/NO_x and C_2H_2/NO_x analyses of the Los Angeles data[32] showed significant deviations on high oxidant days. Since the same types of questions have appeared in laboratory experiments, it seems that a greater latitude of nitrogen-bearing compounds should be sought in future atmospheric studies.

The plans announced for an APCO regional study should hold many of the solutions to the problems identified here. Conversely, application of the model should provide valuable feedback to such programs. Clarifications in the chemical mechanism should take the form of better values of rate constants for the controlling reactions. Perhaps the very selection of which reactions to include might be altered for the air contaminant hydrocarbon mix. Mathematical techniques seem well enough advanced to match the simpler formulations of photochemical modeling schemes to the computing machinery available. The more complex schemes proposed recently will continue to shed light on questions of dispersion parameters and inventory accuracy.

Continued use of the model we have developed should generalize it to a point where it can be integrated in the process of implementation planning. The job ahead is a difficult one and only a judicious mixture of experimental and theoretical effort will lead to a useful tool that is consistent with the requirements facing us now.

REFERENCES

1. A. Q. Eschenroeder and J. R. Martinez, A Modeling Study to Characterize Photochemical Atmospheric Reactions to the Los Angeles Basin Area, General Research Corporation CR-1-152, November 1969.

2. R. C. Wanta, "Meteorology and Air Pollution," Air Pollution, Vol. 1, 2nd ed., A.C. Stern, Ed., Academic Press, New York, 1968, Ch. 7.

3. H. Moses, Mathematical Urban Air Pollution Models, Paper 69-31 62nd Annual Meeting of the Air Pollution Control Association, New York, N.Y., June 1969.

4. J. H. Seinfeld, Mathematical Models of Air Quality Control Regions, Symposium on the Development of Air Quality Standards, Los Angeles, Calif., October 1969.

5. S. Calvert, "A Simulation Model for Photochemical Smog," California Air Environment, Vol. 1, No. 3, Jul-Sep 1969, pp. 1-3.

6. L. Wayne, R. Danchick, M. Weisburd, A. Kokin, and A. Stein, Modeling Photochemical Smog on a Computer for Decision-Making, Paper 70-18, Air Pollution Control Association 63rd Annual Meeting, St. Louis, Mo., June 14-19, 1970.

7. S. K. Friedlander and J. H. Seinfeld, "A Dynamic Model of Photochemical Smog," Environmental Science and Technology, Vol. 3, No. 11, November 1969, pp. 1175-1182.

8. R. C. Sklarew, A New Approach: The Grid Model of Urban Air Pollution, Air Pollution Control Association Paper 70-79, 63rd Annual Meeting, St. Louis, Missouri, June 14-18, 1970.

9. P. Roth, Development of a Simulation Model for Estimating Photochemical Pollutants, Presentation at an Information Meeting of Atmospheric Diffusion Modeling Studies by NAPCA Contractors, Raleigh, N.C., November 16-17, 1970.

10. A. P. Altshuller and J. J. Bufalini, "Photochemical Aspects of Air Pollution: A Review," Photochemistry and Photobiology, Vol. 4, 1965, pp. 97-146.

Preceding page blank

REFERENCES (Cont.)

11. E. A. Schuck and G. J. Doyle, Photooxidation of Hydrocarbons in Mixtures Containing Oxides of Nitrogen and Sulfur Dioxide, Air Pollution Foundation Report No. 29, San Marino, Calif., October 1959.

12. D. H. Stedman, E. D. Morris, Jr., E. E. Daby, H. Niki, and B. Weinstock, The Role of OH Radicals in Photochemical Smog, American Chemical Society Division of Water Air and Waste Chemistry, Chicago, Illinois, September 13-18, 1970.

13. J. R. Holmes, A. D. Sanchez, and A. H. Bockian, Atmospheric Photochemistry: Some Factors Affecting the Conversion of NO to NO_2, Pacific Conference on Chemistry and Spectroscopy, San Francisco, October 6-9, 1970.

14. K. Westberg and N. Cohen, The Chemical Kinetics of Photochemical Smog as Analyzed by Computer, AIAA Third Fluid and Plasma Dynamics Conference Paper No. 70-753, Los Angeles, June 29-July 1, 1970.

15. A. P. Altshuller, S. L. Kopczynski, W. A. Lonneman, T. L. Becker, and R. Slater, "Chemical Aspects of the Photooxidation of the Propylene-Nitrogen Oxide System," Environmental Science and Technology, Vol. 1, No. 11, Nov. 1967, pp. 899-914.

16. A. P. Altshuller, and J. J. Bufalini, "Photochemical Aspects of Air Pollution: A Review," Environmental Science and Technology, Vol. 5, No. 5, January 1971, pp. 39-64.

17. J. H. Seinfeld, private communication, letter dated June 2, 1970.

18. A. P. Altshuller, S. L. Kopczynski, D. Wilson, W. Lonneman, and F. D. Sutterfield, "Photochemical Reactivities of n-Butane and Other Paraffinic Hydrocarbons," Journal of the Air Pollution Control Assoc., Vol. 19, No. 10, October 1969, pp. 787-790.

19. M. W. Korth, A. H. Rose, Jr., and R. C. Stahman, "Effects of Hydrocarbon to Oxides of Nitrogen Ratios on Irradiated Auto Exhaust, Part 1," Journal of the Air Pollution Control Assoc., Vol. 14, No. 5, May 1964, pp. 168-175.

20. W. G. Agnew, "Automotive Air Pollution Research," Proc. Roy. Soc., Series A, Vol. 307, 1968, pp. 153-181. (Data reproduced from APCA paper by C. S. Tuesday, B. A. D'Alleva, J. M. Heuss, and G. J. Nebel, June 1967).

REFERENCES (Cont.)

21. J. Heicklen, K. Westberg, and N. Cohen, The Conversion of NO to NO_2 in Polluted Atmospheres, Pennsylvania State University Center for Air Environment Studies Publication 115-69, July 1969.

22. K. Westberg, N. Cohen, and K. W. Wilson, "Carbon Monoxide: Its Role in Photochemical Smog Formation," Science, Vol. 171, March 12, 1971, pp. 1013-1015.

23. W. F. Ames, Nonlinear Partial Differential Equations in Engineering, N.Y. Academic Press, 1965, pp. 341-342.

24. R. S. Varga, "On Higher Order Stable Implicit Methods for Solving Parabolic Partial Differential Equations," J. Math and Physics, Vol. 40, 1961, pp. 220-231.

25. D. Magnus and H. Schecter, Analysis and Application of the Padé Approximation for the Integration of Chemical Kinetic Equations, Technical Report 642, General Applied Science Laboratories, Inc., 1967.

26. S. S. Wu, "A Study of Heat Transfer Coefficients in the Lowest 400 meters of the Atmosphere," Journal of Geophysical Research, Vol. 70, No. 8, April 15, 1965, pp. 1801-1807.

27. C. R. Hosler, "Vertical Diffusivity from Radon Profiles," Journal of Geophysical Research, Vol. 74, No. 28, December 20, 1969, pp. 7018-7026.

28. G. De Zorzi, "Applicazione della Equazione di Diffusione allo Studio della Bassa Atmosfera," Rivista di Meteorologica Aeronautica, Vol. 30, No. 1, March 1970, pp. 3-28.

29. Atmospheric Reaction Studies in the Los Angeles Basin, Vols. I-IV, Scott Research Laboratories, February 1970.

30. Final Report on Phase I, Atmospheric Reaction Studies in the Los Angeles Basin, Vols. I and II, Scott Research Laboratories, June 30, 1969.

31. Monitoring Data from Los Angeles County Air Pollution Control District, 1969.

REFERENCES (Cont.)

32. A. Q. Eschenroeder and J. R. Martinez, Analysis of Los Angeles Atmospheric Reaction Data from 1968 and 1969, General Research Corporation CR-1-170, July 1970.

33. A. Q. Eschenroeder, Some Preliminary Air Pollution Estimates for the Santa Barbara Region 1970-1990, General Research Corporation IMR-1278, March 1970.

34. H. Johnston, "Reaction in the Atmosphere," Project Clean Air Task Force Assessments, Vol. 4, Task Force No. 7, Section 3, University of California, September 1, 1970, p. 3-1.